A rationally designed NRP1-independent superagonist SEMA3A mutant is an effective anticancer agent

A rationally designed NRP1-independent superagonist SEMA3A mutant is an effective anticancer agent

Noemi Gioelli[1,2,*], Federica Maione[2,3,*], Chiara Camillo[1,2], Michela Ghitti[4], Donatella Valdembri[1,2], Noemi Morello[5], Marie Darche[6], Lorena Zentilin[7], Gabriella Cagnoni[1,2], Yaqi Qiu[2,3], Mauro Giacca[7], Maurizio Giustetto[5,8], Michel Paques[9,10], Ilaria Cascone[6], Giovanna Musco[4], Luca Tamagnone[1,2,†], Enrico Giraudo[2,3,†,‡] and Guido Serini[1,2,†,‡]

[1]Department of Oncology, University of Torino School of Medicine, 10060 Candiolo, Torino, Italy.
[2]Candiolo Cancer Institute, FPO-IRCCS, 10060 Candiolo, Torino, Italy.
[3]Department of Science and Drug Technology, University of Torino, 10125 Torino, Italy.
[4]Biomolecular NMR Unit, IRCCS Ospedale San Raffaele, 20132 Milano, Italy.
[5]Department of Neuroscience, University of Torino School of Medicine, 10126 Torino, Italy.
[6]Growth, Reparation and Tissue Regeneration Laboratory, ERL-CNRS 9215, University of Paris-Est, 94000 Créteil, France.
[7]Molecular Medicine Laboratory, International Centre for Genetic Engineering and Biotechnology, 34149 Trieste, Italy.
[8]National Institute of Neuroscience-Italy, 10126 Torino, Italy.
[9]Vision Institute, Sorbonne University, UPMC University of Paris 06, INSERM, CNRS, 75012 Paris, France.
[10]Centre Hospitalier National d'Ophtalmologie des Quinze-Vingts, INSERM-DHOS CIC 503, 75012 Paris, France.

‡Corresponding author. Email: guido.serini@ircc.it (G.S.); enrico.giraudo@ircc.it (E.G.)
* These authors contributed equally to this work as first authors.
† These authors contributed equally to this work as senior authors.

Article

This article has a correction. Please see:

Erratum for the Research Article: "A rationally designed NRP1-independent superagonist SEMA3A mutant is an effective anticancer agent" by N. Gioelli, F. Maione, C. Camillo, M. Ghitti, D. Valdembri, N. Morello, M. Darche, L. Zentilin, G. Cagnoni, Y. Qiu, M. Giacca, M. Giustetto, M. Paques, I. Cascone, G. Musco, L. Tamagnone, E. Giraudo, G. Serini - July 25, 2018

Semaphoring to tumor vasculature

Solid tumors typically have blood vessels that are not only increased in number but also exhibit various structural and functional abnormalities. Thus, vascular normalization is frequently proposed as an antitumor strategy, with the goal of improving intratumoral oxygenation and drug delivery. SEMA3A, a protein from the semaphorin family, is a known vascular normalizing agent but not a good therapeutic candidate due to adverse effects. To address this concern, Gioelli et al. engineered a mutant version of SEMA3A that retained its vascular normalizing function but did not activate the pathway responsible for the main side effects. The authors then confirmed the ability of mutant SEMA3A to normalize tumor vasculature and demonstrated its anticancer effects alone and combined with chemotherapy.

Abstract

Vascular normalizing strategies, aimed at ameliorating blood vessel perfusion and lessening tissue hypoxia, are treatments that may improve the outcome of cancer patients. Secreted class 3 semaphorins (SEMA3), which are thought to directly bind neuropilin (NRP) co-receptors that, in turn, associate with and elicit plexin (PLXN) receptor signaling, are effective normalizing agents of the cancer vasculature. Yet, SEMA3A was also reported to trigger adverse side effects via NRP1. We rationally designed and generated a safe, parenterally deliverable, and NRP1-independent SEMA3A point mutant isoform that, unlike its wild-type counterpart, binds PLXNA4 with nanomolar affinity and has much greater biochemical and biological activities in cultured endothelial cells. In vivo, when parenterally administered in mouse

models of pancreatic cancer, the NRP1-independent SEMA3A point mutant successfully normalized the vasculature, inhibited tumor growth, curbed metastatic dissemination, and effectively improved the supply and anticancer activity of chemotherapy. Mutant SEMA3A also inhibited retinal neovascularization in a mouse model of age-related macular degeneration. In summary, mutant SEMA3A is a vascular normalizing agent that can be exploited to treat cancer and, potentially, other diseases characterized by pathological angiogenesis.

INTRODUCTION

Blood vessels of most solid cancers exhibit structural and functional abnormalities that severely hamper antineoplastic drug delivery and radiotherapy effectiveness (1). Moreover, the hypoxia resulting from impaired vascular perfusion supports the maintenance of tumor-initiating cancer stem cells (2, 3) and triggers proinvasive and immunosuppressive gene transcription programs that foster cancer progression (4, 5). The functional impact of cancer genome mutations and transcriptional alterations highly depends on environmental selection pressures (6), such as poor tissue oxygenation. In their aiming at relieving stress factors that affect the selection process and thus foster cancer aggressiveness, pharmacological strategies such as vascular normalization (1) may thus complement conventional treatments. In particular, improving cancer perfusion and oxygenation can favor the delivery of chemotherapies, increase the sensitivity to radiation therapy, and impair metastatic dissemination along with cancer stem cell renewal (1).

Semaphorins (SEMA) are a large family of extracellular signals controlling axonal navigation and endothelial cell (EC) migration in development, as well as tumor angiogenesis, cancer progression, and immune function in adulthood (7–9). We previously showed how homodimeric secreted chemorepulsive class 3 SEMA3A is a physiological vascular normalizing factor (10) that is present in precancerous lesions of multiple preclinical transgenic mouse models of cancer but lost during cancer progression (11, 12). When reintroduced by gene transfer, SEMA3A successfully counteracted cancer blood vessel abnormalization and metastatic dissemination (11–13). Accordingly, decreased SEMA3A protein expression has been correlated with poor prognosis in human gastric (14), hepatocellular (15), prostatic (16), and squamous cell carcinomas (17), as well as meningiomas (18). In addition, integrated genomic and transcriptional analyses of a wide cohort of human pancreatic ductal adenocarcinomas (PDACs) identified SEMA3A gene as transcriptional target that is strongly down-regulated by N-terminally truncated p63 (TP63ΔN) in squamous PDAC, a molecular subtype that is an independent poor prognostic factor (19).

Neuropilin 1 (NRP1) and sema domain–containing type A plexins (PLXNAs) are considered to be the mandatory ligand-binding and signal-transducing components of SEMA3A holoreceptors, respectively (7). In this regard, a caveat is that SEMA3A was also reported to mediate some adverse side effects via the NRP1 receptor subunit. These included the attraction of protumoral macrophages (20) and increased vascular permeability when SEMA3A protein was administered acutely (21, 22), thus conceivably exposing vascular ECs to high amounts of this chemorepellent.

Here, we describe a safe, effective, and parenterally deliverable SEMA3A mutant isoform, which, unlike its wild-type counterpart, directly binds to PLXNA4 with high affinity but cannot interact with NRP1. Owing to its ability to avidly bind to PLXNA4, the new SEMA3A mutant displays stronger activity on ECs in vitro and in vivo in models of pancreatic cancer. Furthermore, we provide evidence that, whereas SEMA3A depends on NRP1 to elicit EC collapse and vascular permeability, NRP1 is fully dispensable to mediate repulsion of migrating ECs, promote vascular normalization, and inhibit tumor growth and dissemination to distant organs.

RESULTS

High-affinity SEMA3A binding to NRP1 is required to elicit EC collapse but not to inhibit haptotactic EC migration

Homodimerization is crucial for the activity of essentially all SEMA proteins (23). From its N to C terminus, the wild-type SEMA3A (SEMA3A_WT) monomer contains a seven-bladed β-propeller sema domain, followed by a plexin-semaphorin-integrin (PSI) domain, an immunoglobulin (Ig)–like domain, and a basic amino acid stretch (7). Noncovalent interactions between sema domains (24) and cysteine disulfide bond(s) lying in the Ig-like domain/basic tail area allow the formation of a stably functional SEMA3A_WT homodimer (25). Furin-like pro-protein convertases cleave the basic stretch, expose a C-terminal arginine, and allow mature SEMA3A_WT to bind with high affinity to the extracellular b1 domain of NRP1

(8, 26). The extracellular a1 domain of NRP1 is instead posited to stabilize an extremely weak (27), albeit functionally relevant (28) canonical interaction between the sema domains of SEMA3A_WT and PLXNAs. Furin-like proteases also sever mature SEMA3A_WT just downstream of its PSI domain, thus physically dissociating the sema/PSI domain and Ig-like domain/basic tail regions (29); this cleavage terminates SEMA3A_WT interaction with NRP1 (8, 26).

Because full-length SEMA3A_WT can cause adverse side effects through NRP1 (20, 21, 30), but it was recently postulated to directly, although tenuously, bind PLXNAs as well (Fig. 1A) (20, 27, 28), we asked whether SEMA3A actually requires binding to NRP1 to control EC behavior. First, we generated a mutant SEMA3A lacking the Ig-like domain and C-terminal basic stretch (SEMA3A_ΔIg-b; Fig. 1A), two moieties that are well known to mediate high-affinity SEMA3A binding to NRP1 [see (8, 26) and references therein]. To make the remaining sema-PSI region (amino acids 1 to 548) of mutant SEMA3A_ΔIg-b stably dimeric and easily purifiable on Sepharose protein A, we fused its C terminus with the mouse IgG1 constant fragment (Fig. 1A and fig. S1).

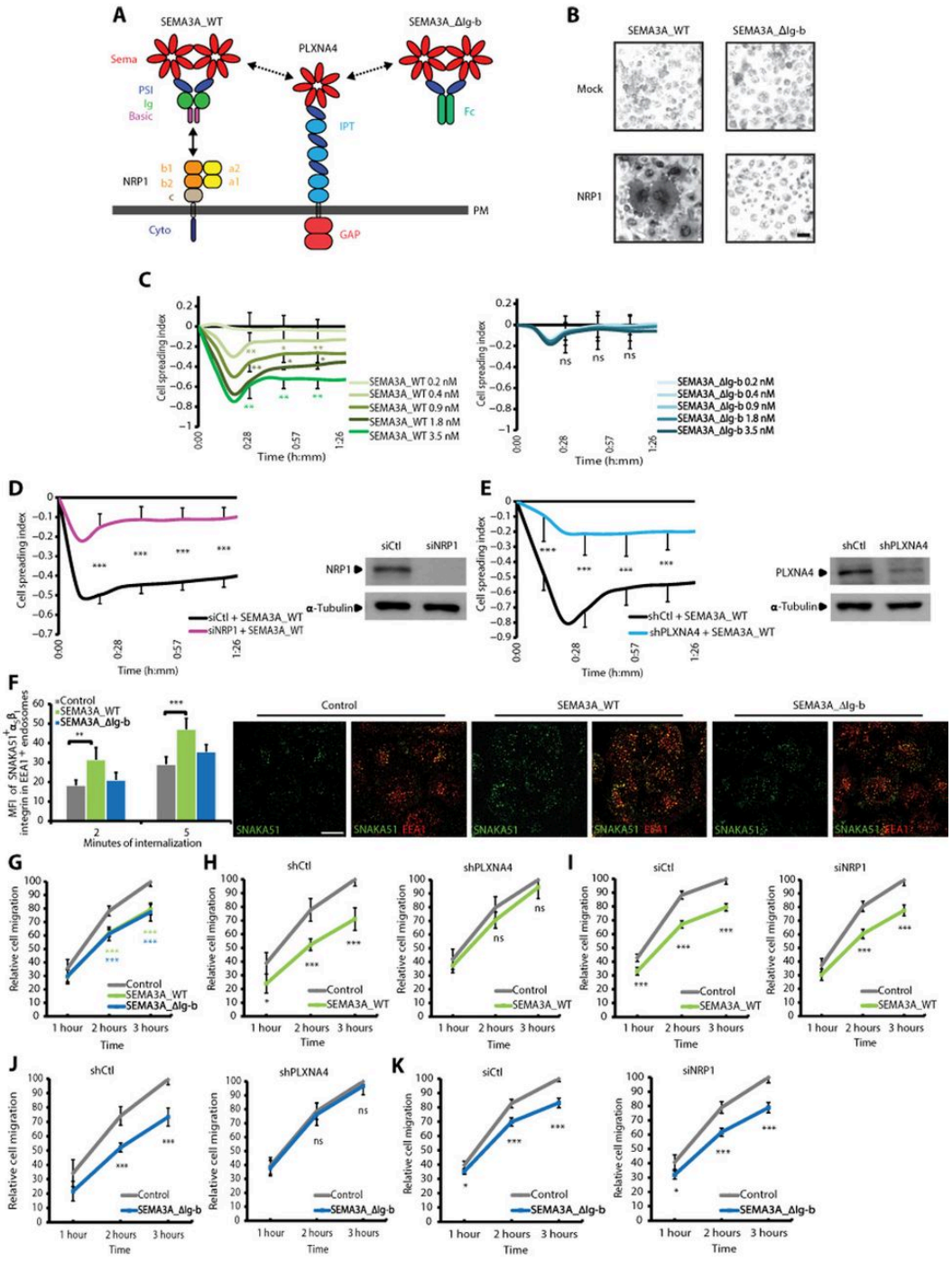

Fig. 1. Unlike PLXNA4, NRP1 is necessary for SEMA3A-elicited EC collapse but not for SEMA3A inhibition of EC haptotaxis.

(A) The C-terminal basic stretch of SEMA3A_WT binds the b1 domain of NRP1 with high-affinity (solid double arrow) NRP1, and this domain acts as a co-receptor that keeps SEMA3A_WT close to PLXNA4. SEMA3A_WT drives the activation of PLXNA4 guanosine triphosphatase (GTPase) activating protein (GAP) domain via a very low-affinity sema domain–sema domain interaction (dashed double arrow). The SEMA3A_ΔIg-b deletion mutant lacks the high-affinity NRP1-binding basic stretch and, after fusion with the mouse IgG1 constant fragment (Fc), is stably dimeric. Cyto, cytosolic domain; IPT, integrin-plexin-transcription factor domain; PM, plasma membrane. (B) In situ binding assays on NRP1 or green fluorescent protein (Mock)–transfected COS-7 cells evaluated the ability of AP-SEMA3A_WT and mutant AP-SEMA3A_ΔIg-b to bind to NRP1. Scale bar, 50 μm. (C) Real-time analysis of SEMA3A-elicited EC collapse as evaluated by an xCELLigence system. ECs were left to adhere on type I collagen (Coll I) for 2 hours. Different amounts (0.2 to 3.5 nM) of either SEMA3A_WT (green) or SEMA3A_ΔIg-b (blue) were then added or not to ECs, and cell spreading index was monitored over time. A representative experiment out of three is shown. For simplicity, data from the same experiment are plotted in two separate graphs: SEMA3A_WT (left graph) and SEMA3A_ΔIg-b (right graph). Each curve is the mean of three technical replicates ± SD. (D and E) Collapse of control (siCtl or shCtl), NRP1 (siNRP1)–silenced (D), or PLXNA4 (shPLXNA4)–silenced (E) ECs was analyzed over time upon addition of 3.5 nM SEMA3A_WT. A representative experiment out of six (D) or five (E) is depicted. Results are the mean of four technical replicates ± SD. (F) To label ligand-bound/active $\alpha_5\beta_1$ integrins on the cell surface, living ECs were incubated for 10 min at 37°C with SNAKA51 mAb. ECs were then left to internalize SNAKA51-bound $\alpha_5\beta_1$ integrins for 2 or 5 min either in the absence (control; gray) or in the presence of SEMA3A_WT (green) or SEMA3A_ΔIg-b (blue). After acid wash at 4°C, ECs were fixed and immunostained to visualize the early endosome marker early endosome antigen 1 (EEA1) (red in merge) and endocytosed SNAKA51–$\alpha_5\beta_1$integrin complexes (green). Representative single confocal z sections of ECs that were incubated for 5 min are shown. Mean fluorescence intensity (MFI) of SNAKA51 mAb accumulated in EEA1$^+$ endosomes in six randomly chosen fields (≥18 cells per field) for each experimental point, from two independent experiments, was acquired at the same acquisition settings and quantified by ImageJ software. Scale bar, 20 μm. (G) Real-time analysis of haptotactic EC migration toward Coll I either in the absence (control, gray) or in the presence of 3.5 nM SEMA3A_WT (green) or SEMA3A_ΔIg-b (blue), assessed with an xCELLigence system. Results are the mean ± SEM of three independent experiments, with each experimental point performed in triplicate. (H to K) Haptotactic migration toward Coll I of control (shCtl or siCtl), PLXNA4(shPLXNA4)–silenced (H and J), or NRP1 (siNRP1)–silenced (I and K) ECs was analyzed over time either in the absence (control, gray) or in the presence of 3.5 nM SEMA3A_WT (green) (H and I) or SEMA3A_ΔIg-b (blue) (J and K). For simplicity, data from the same experiments are plotted in two separate graphs: shCtl (H and J) or siCtl (I and K) (left graphs) and shPLXNA4 (H and J) or siNRP1 (I and K) (right graph). Results are the mean ± SEM of three (H and J), four (K), or five (I) independent experiments, with each experimental point having been performed in triplicate. Results were analyzed by a two-tailed heteroscedastic Student's t test; ns, not significant; *P < 0.05, **P < 0.01, and ***P < 0.001.

Consistent with previous reports (8, 26), ligand-receptor in situ binding assay on COS-7 cells demonstrated that alkaline phosphatase (AP)–conjugated SEMA3A_WT, but not AP-SEMA3A_ΔIg-b, interacts with NRP1 with high affinity (Fig. 1B). Next, we compared the ability of equimolar amounts of affinity-purified Fc-tagged SEMA3A_WT and SEMA3A_ΔIg-b to induce the collapse of adherent ECs (31) and quantitatively monitored it in real time through an impedance-based cell collapse assay (32). As confirmation of the role of NRP1 in the holoreceptor complex, we found that SEMA3A_WT, but not SEMA3A_ΔIg-b, elicits a robust retraction of cultured human umbilical artery ECs (Fig. 1C). Consistent with that, we also observed that NRP1 silencing (33) severely hampers the activity of SEMA3A_WT in causing the collapse of ECs (Fig. 1D). PLXNA4 is a major SEMA3A signaling receptor in both neurons (34) and ECs (35); accordingly, PLXNA4 silencing hindered the EC collapse triggered by SEMA3A_WT (Fig. 1E). Together, our data confirmed that NRP1 and PLXNA4 are both essential for SEMA3A_WT to trigger EC collapse.

In ECs, NRP1 localizes at extracellular matrix (ECM) adhesions, where it drives the internalization of active/ECM-bound $\alpha_5\beta_1$ integrin, as recognized by SNAKA51 monoclonal antibody (mAb) (33). In addition, the binding of NRP1 b1 domain to the C-terminal basic tail of SEMA3A is sufficient to stimulate macropinocytosis (36), and SEMA3E-elicited EC collapse depends on integrin internalization (37). Therefore, we investigated whether SEMA3A may promote active/ECM-bound $\alpha_5\beta_1$ integrin endocytosis in ECs via NRP1. SNAKA51 mAb was preincubated for 10 min on living ECs, which were then washed and incubated for different amounts of time in the absence or presence of equimolar amounts of SEMA3A_WT or SEMA3A_ΔIg-b. Next, surface-bound nonendocytosed SNAKA51 was removed by acid wash, and the colocalization between endocytosed SNAKA51$^+$ $\alpha_5\beta_1$ integrins and EEA1$^+$ vesicles was analyzed by confocal fluorescence microscopy

and quantified (Fig. 1F). We found that SEMA3A_WT, but not SEMA3A_ΔIg-b, effectively stimulated SNAKA51$^+$ $\alpha_5\beta_1$ integrin internalization in EEA1$^+$ early endosomes. Thus, the binding of the Ig-like domain/basic tail region of SEMA3A to NRP1 is crucial to promote the endocytosis of active integrins from ECM adhesions and to favor EC collapse, potentially due to retraction of disentangled cellular processes.

In addition to mediating stable adhesion, integrin-ECM interactions are required for the active protrusion of the leading membrane in cell migration. Thus, through a real-time impedance-based haptotaxis assay, we quantitatively compared the ability of equimolar amounts of affinity-purified Fc-tagged SEMA3A_WT and SEMA3A_ΔIg-b to inhibit the migration of ECs toward ECM proteins, such as Coll I (33). Notably, SEMA3A_ΔIg-b was as efficient as SEMA3A_WT in inhibiting EC directional migration toward Coll I (Fig. 1G). Moreover, we observed that the inhibitory activity of both SEMA3A_WT (Fig. 1, H and I) and SEMA3A_ΔIg-b (Fig. 1, J and K) on Coll I–driven EC haptotaxis was abrogated by PLXNA4 (Fig. 1, H and J) but not by NRP1 (Fig. 1, I and K) silencing. Together, our findings indicate that, unlike EC collapse, the inhibition of haptotactic EC migration by SEMA3A does not require high-affinity NRP1 binding but relies on PLXNA4 signaling.

High-affinity SEMA3A binding to NRP1 is required to elicit in vivo vascular permeability but not to inhibit tumor growth

C-end rule peptides, which mimic the C-terminal arginine-containing sequences of native vascular endothelial growth factor A (VEGF-A) (30) and furin-activated mature SEMA3A_WT basic stretches (36), induce EC internalization and vascular leakage by binding the extracellular b1 domain of NRP1 (30, 36). Therefore, we assessed whether NRP1 binding may be essential to mediate blood vessel permeability elicited by acute administration of different SEMA3A protein isoforms. To this end, first, we intradermally injected mouse ears with SEMA3A_WT, SEMA3A_ΔIg-b, or VEGF-A. Next, we measured vascular leakage in Miles assays (38) by intravenously inoculating the azo dye Evans Blue, which binds to albumin with high affinity, and measuring the amount of extravasated dye. VEGF-A and, to a lesser extent, SEMA3A_WT, but not SEMA3A_ΔIg-b, fostered Evans Blue extravasation (Fig. 2, A and B), thus indicating the dependency of SEMA3A-induced vascular leakage on NRP1 binding.

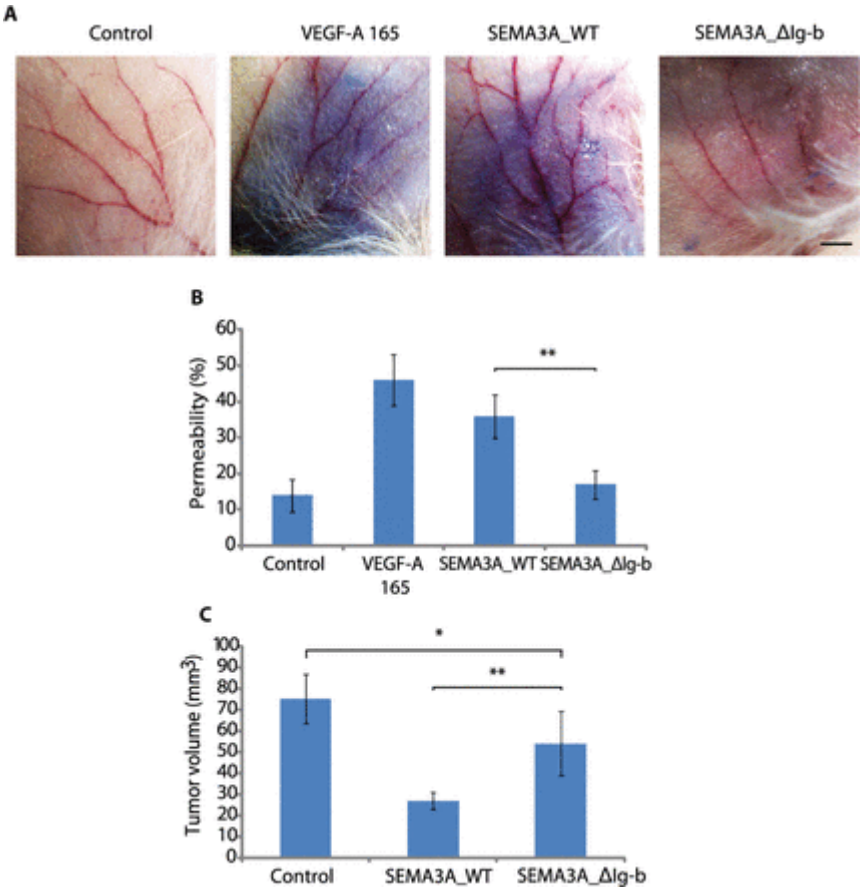

Fig. 2SEMA3A_ΔIg-b does not induce vascular permeability and slightly reduces tumor growth in RIP-Tag2.

(A) Representative images showing Evans Blue extravasation from the mouse ear vasculature upon acute stimulation with 600 ng of recombinant SEMA3A_WT, SEMA3A_ΔIg-b, or VEGF-A 165, used as a positive control (n = 3 per group). Saline solution was used as a negative control (from here on, referred to as "control"). Scale bar, 1 mm. (B) Permeability was evaluated as the percentage of leaked blue/total area (mm^2). SEMA3A_WT, but not SEMA3A_ΔIg-b, elicited vascular leakage. (C) Total tumor volume of RIP-Tag2 mice treated for 4 weeks with AAV8-SEMA3A_WT or AAV8-SEMA3A_ΔIg-b. Results are the mean ± SD (n = 5 per group). Results were analyzed by nonparametric two-tailed, unpaired Mann-Whitney U test; *P < 0.05 and **P < 0.01.

Then, we evaluated whether the antitumor effects of SEMA3A may also depend on NRP1 binding. For this purpose, we used the transgenic RIP-Tag2 pancreatic neuroendocrine tumor (PNET) mouse model, in which we previously observed that SEMA3A_WT gene delivery by means of adeno-associated virus-8 (AAV8) successfully impaired tumor growth and metastatic dissemination (12, 13). We transduced tumor-bearing RIP-Tag2 mice with control AAV8, AAV8-SEMA3A_WT, or AAV8-SEMA3A_ΔIg-b, and we compared their effects on tumor volume after 4 weeks. AAV8-SEMA3A_WT reduced tumor volume by 64% compared to control, whereas AAV8-SEMA3A_ΔIg-b only decreased tumor burden by 29% (Fig. 2C). Similarly, intraperitoneal administration of recombinant SEMA3A_ΔIg-b protein at 3 mg/kg three times per week for 4 weeks induced a 28% inhibition of tumor growth in RIP-Tag2 mice (fig. S2). Although SEMA3A_ΔIg-b was less efficient than SEMA3A_WT in hampering the growth of RIP-Tag2 PNETs, these findings revealed that the antitumor activity of SEMA3A does not necessarily depend on NRP1 but may be mediated by other signaling receptors, such as PLXNA4 (34, 35).

In silico analyses unveil a key role of extrusion 1 in controlling SEMA3A binding to PLXNA4

To enhance the anticancer properties of NRP1-independent SEMA3A_ΔIg-b, we sought to increase its affinity for PLXNAs by a rationally designed mutagenesis approach. To identify the amino acids responsible for the head-to-head heterodimeric interactions between SEMA and PLXNA sema domains (28, 39), we first analyzed the high-resolution crystallographic structure of the SEMA6A-PLXNA2 complex (Protein Data Bank code: 3oky) (39), which we considered as a faithful template to define the SEMA-PLXN interface. To account for conformational rearrangements occurring in solution and to identify the contacts that stably participate to complex formation, we performed all-atom classical molecular dynamics simulations in explicit water. Analysis of the simulations revealed an extended densely packed hydrophobic interface stabilized by few hydrophilic interactions. Because long-range electrostatic forces are crucial in protein-protein recognition, and surface charge complementarity supports the formation and lifetime of protein complexes (40), we focused on the electrostatic contacts occurring at the interface between SEMA6A and PLXNA2 sema domains (Fig. 3A and table S1). In particular, besides the conserved involvement of the β3D-β4A loop (28, 39), we examined the hydrophilic interactions encompassing the so-called extrusions (fig. S3), two structural peculiarities of the sema fold β-propeller topology that conceivably acquired functional roles during evolution (41). We observed the following: (i) the presence of a stable salt bridge between $K110_{SEMA6A}$ and $D408_{PLXNA2}$, located on extrusion 1 of SEMA6A and extrusion 2 of PLXNA2, respectively (Fig. 3A, right inset); (ii) the formation of a salt bridge between the guanidinium group of $R267_{SEMA6A}$ and the carboxylic group of $E105_{PLXNA2}$located on loop β4C-β4D of SEMA6A and extrusion 1 of PLXNA2, respectively (Fig. 3A, left inset). Thus, we reasoned that SEMA3A-driven activation of PLXNA4 could be strengthened by designing a SEMA3A mutant with empowered charge complementarity contacts within this electrostatic interaction interface. We noticed that in extrusions 1 and 2, PLXNA4 has two acidic residues, E102 and D404 (corresponding to E105 and D408 in PLXNA2; fig. S4), which might potentially establish electrostatic interactions with SEMA3A. In its β4C-β4D loop, in the position equivalent to R267 of SEMA6A, SEMA3A displays a basic amino acid residue ($R277_{SEMA3A}$) that might be suitable for interactions with E102 of PLXNA4 extrusion 1 (fig. S4). However, on the opposite edge of the electrostatic interface, SEMA3A extrusion 1 contains an alanine ($A106_{SEMA3A}$) that cannot engage in electrostatic interactions (fig. S4). Thus, we theorized that the substitution of SEMA3A_A106 with a charged residue (for example, a lysine) might create an additional complete charge complementarity between SEMA3A extrusion 1 and PLXNA4 extrusion 2, eventually increasing the interactions between these two sema domains. To start testing this hypothesis, we created an in silico model of A106K-mutated SEMA3A (SEMA3A_A106K)–PLXNA4 complex, which was

subsequently relaxed by all-atoms molecular dynamics simulations in explicit solvent. The complex was stable all along the simulation (fig. S5), and the highest fluctuations were located mostly in unstructured regions of both proteins (figs. S6 and S7). We observed that the SEMA3A_A106K-PLXNA4 interface is composed of a combination of hydrophobic and hydrophilic interactions. An analysis of the electrostatic interface along the simulation supported the charge complementarity hypothesis (Fig. 3B and table S1); in particular, extrusion 1 of SEMA3A_A106K and extrusion 2 of PLXNA4 are engaged in an extended network of hydrophilic interactions, whereby $D404_{PLXNA4}$ establishes both a salt bridge with $R166_{SEMA3A}$ and a water-mediated interaction with $K106_{SEMA3A\_A106K}$, thus supporting a relevant contribution of a basic residue in this position (Fig. 3B, right inset). However, the identity of the amino acids mediating the interaction between SEMA extrusion 1 and PLXN extrusion 2, as well as SEMA β2D-β3A loop and PLXN extrusion 2/bulge, is completely different in SEMA6A-PLXNA2 and SEMA3A-PLXNA4 interfaces. A stable H-bond between the backbone of $W105_{SEMA3A\_A106K}$ and that of $L393_{PLXNA4}$ also contributes to interdomain interactions in this region (Fig. 3B, right inset), and it is absent in the SEMA6A-PLXNA2 complex (Fig. 3A, right inset, and table S1). Notably, overall, the network of interactions with PLXNA4 extrusion 2 is more effective in SEMA3A_A106K as compared to the SEMA6A-PLXNA2 interaction (Fig. 3 and table S1). Moreover, in stark difference to SEMA6A-PLXNA2 interaction (Fig. 3A, main image and left inset), we did not find any stable electrostatic contact between extrusion 1 of PLXNA4 and SEMA3A_A106K (Fig. 3B, main image and left inset, and fig. S4B), most likely because of the different length of the β4C-β4D loop of SEMA3A, which is shorter than the corresponding loop in SEMA6A. As a consequence, $R277_{SEMA3A}$ is not at the proper distance to create stable interactions with acidic residues of the extrusion 1 of PLXNA4; it is therefore conceivable that electrostatic contacts in this region are not reproduced in the SEMA3A_A106K-PLXNA4 complex (Fig. 3B, left inset, and table S1). By contrast, our simulations support the contribution of extrusion 1 of SEMA3A to the binding with PLXNs, whereby mutations within this region of SEMA3A may tune its binding affinity. In general, our analysis also suggests that SEMA of different subclasses, such as SEMA6A and SEMA3A, establish the electrostatic binding interface with PLXNA receptors in different ways.

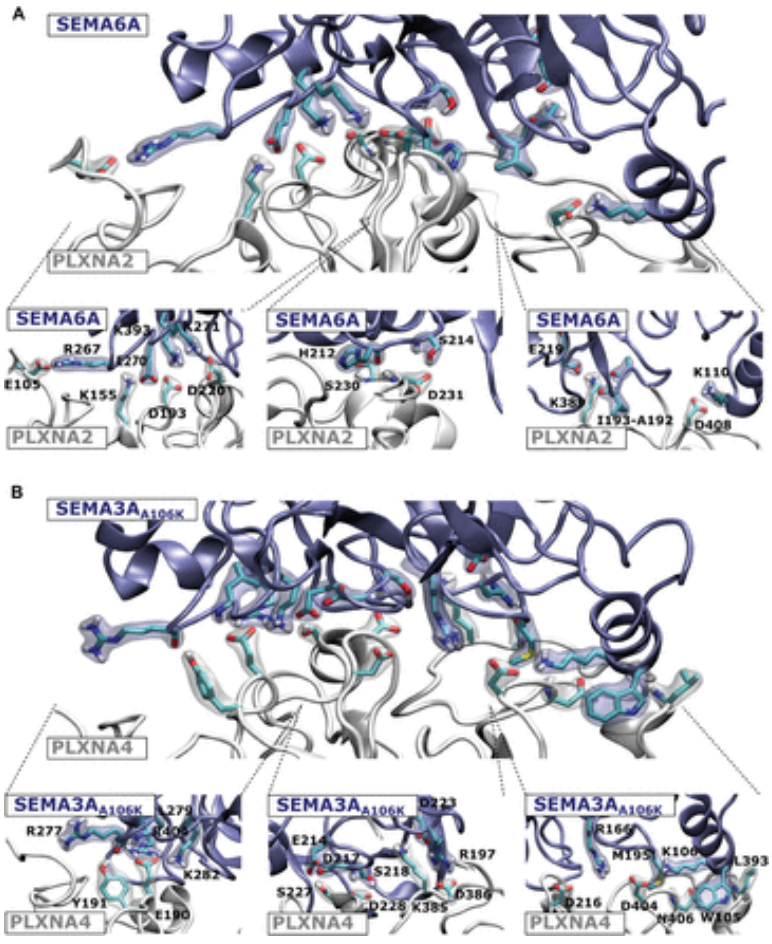

Fig. 3In silico analyses reveal a central role for extrusion 1 in controlling SEMA3A-PLXNA4 molecular interactions.

Representation of the overall electrostatic contacts at the interface of (A) SEMA6A-PLXNA2 and (B) $SEMA3A_{A106K}$-PLXNA4 heterodimers, as determined by molecular dynamics simulations. SEMA and PLXNs are shown as blue and white cartoons, respectively. Residues involved in stable electrostatic interactions (as defined in table S1) are represented as stick and surface models and labeled with the one-letter code in the insets. For clarity, insets are rotated with respect to the corresponding overall representation. All the stick models are shown with carbon, nitrogen, oxygen, sulfur, and hydrogen atoms in cyan, blue, red, yellow, and white, respectively.

SEMA3A_A106K_ΔIg-b mutant is a powerful NRP1-independent PLXNA4 superagonist and EC inhibitor

To provide an experimental validation and quantification of the hypothesized effect of SEMA3A mutagenesis on its binding affinity to PLXNs, we generated a recombinant SEMA3A_A106K_ΔIg-b mutant and assayed the different AP-conjugated SEMA3A variants in ligand-receptor in situ binding assays, as described above. Our results demonstrated that, similar to truncated SEMA3A_ΔIg-b and unlike SEMA3A_WT, SEMA3A_A106K_ΔIg-b mutant cannot interact with NRP1 (Fig. 4A). We then tested the ability of these different AP-tagged constructs to directly bind PLXN family members. We found that, compared to SEMA3A_WT and SEMA3A_ΔIg-b variant (Fig. 4A), the introduction of a single amino acid mutation endowed the SEMA3A_A106K mutant with the ability to bind PLXNA4 with high affinity (Fig. 4B), displaying a dissociation constant (K_d) = 0.7 nM, as estimated by Scatchard plot analysis (Fig. 4C). In comparison, the K_d of SEMA3A_WT binding to NRP1 was 1.1 nM (Fig. 4D), consistent with the literature (42). No other PLXNAs displayed detectable binding to SEMA3A_A106K_ΔIg-b (Fig. 4A), even in the presence of excess NRP1 (fig. S8), thus ruling out the possibility that, in association with NRP1, other PLXNAs may interact with the mutant SEMA3A_A106K_ΔIg-b. To understand whether mutating the homologous $A106_{SEMA3A}$residue into a lysine may increase the binding of other SEMA3s to specific PLXNAs, we mutagenized another antiangiogenic (43) and anticancer (44–48) SEMA3, namely, SEMA3B. We generated, affinity-purified, and tested the ability of Fc-tagged recombinant SEMA3B_ΔIg-b and SEMA3B_A105K_ΔIg-b mutant constructs to directly bind Plexin family members. We found that, compared to SEMA3B_ΔIg-b, SEMA3B_A105K_ΔIg-b bound with very high affinity to PLXNA2 (fig. S9), which is essential for the transduction of SEMA3B, but not of SEMA3A, signals in ECs (49). Thus, it appears that mutating the $A106_{SEMA3A}$ homolog alanine residue into a lysine may increase the binding of SEMA3 proteins other than SEMA3A, such as SEMA3B, to the specific PLXNA receptor that physiologically mediates their signals.

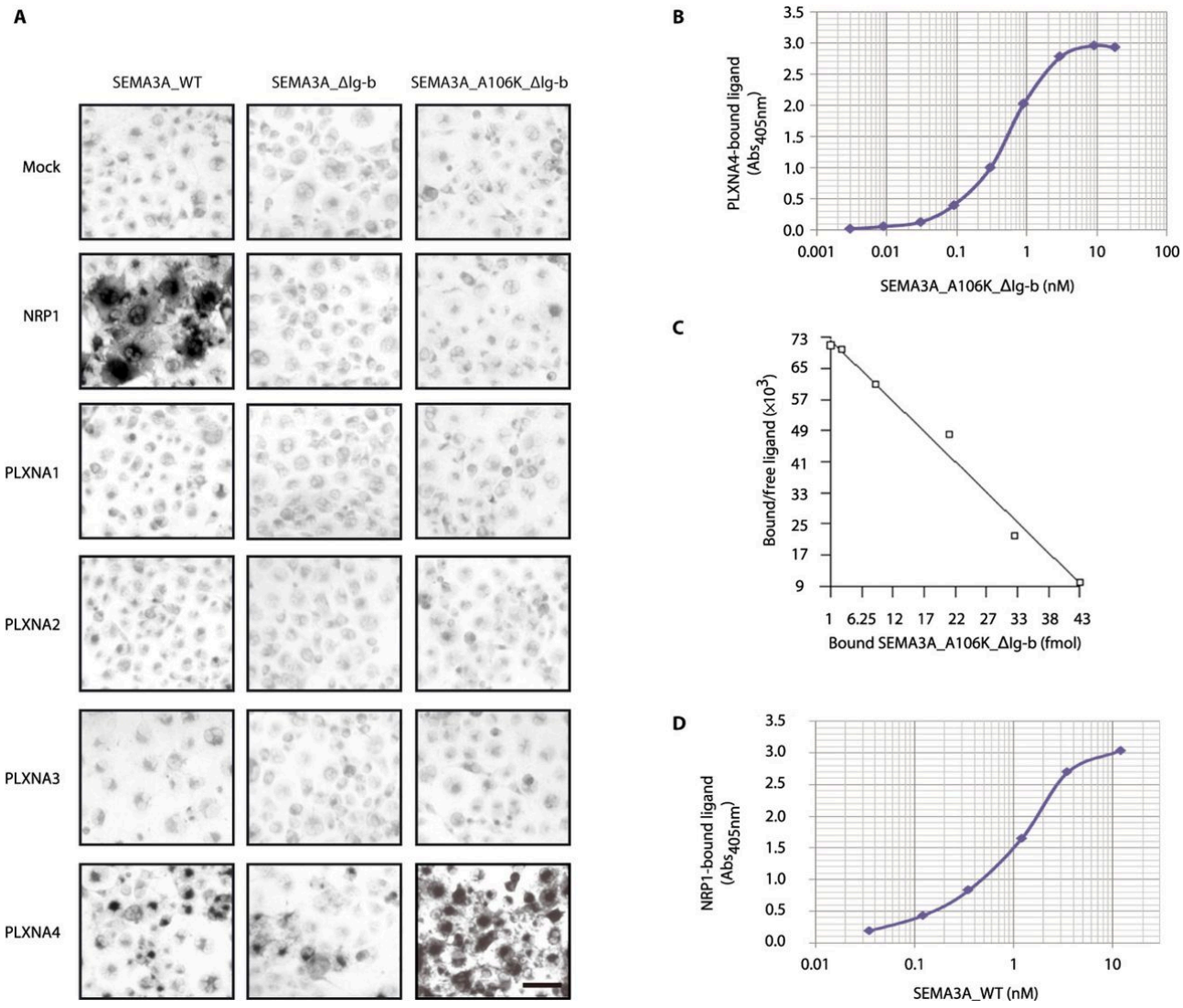

Fig. 4The NRP1-independent SEMA3A_A106K_ΔIg-b mutant protein isoform binds to PLXNA4 with nanomolar affinity.

(A) In situ assays of NRP1, PLXNA1 to PLXNA4, or green fluorescent protein (Mock)–transfected COS-7 cells assessed binding of AP-SEMA3A_WT, AP-SEMA3A_ΔIg-b, and AP-SEMA3A_A106K_ΔIg-b. Scale bar, 100 μm. (B to D) Binding curves (B and D) and Scatchard analysis (C) of PLXNA4 (B and C) or NRP1 (D) at different concentrations of ligands [(B) and (C), SEMA3A_A106K_ΔIg-b; (D), SEMA3A_WT], quantified by spectrometry of chromogenic conversion of AP substrate p-nitrophenyl phosphate. Abs_{405nm}, absorbance at 405 nm.

Next, we generated and affinity-purified Fc-tagged constructs of the different SEMA3A proteins above (fig. S1) and compared the ability of equimolar amounts of Fc-tagged SEMA3A_A106K_ΔIg-b, SEMA3A_ΔIg-b, or SEMA3A_WT to inhibit the haptotactic migration of ECs toward Coll I (Fig. 5). We found that, over a wide concentration range (0.2 to 3.5 nM), Fc-tagged SEMA3A_A106K_ΔIg-b was always much more effective than SEMA3A_ΔIg-b or SEMA3A_WT in inhibiting EC haptotactic migration (Fig. 5, A and B). In accordance with its receptor binding profile, gene silencing experiments also showed that the inhibitory activity of Fc-tagged SEMA3A_A106K_ΔIg-b on EC haptotaxis was dependent on PLXNA4 (Fig. 5C) but not on NRP1 (Fig. 5D). As expected, because SEMA3A requires NRP1 to induce EC collapse (Fig. 1, C and D), but not to inhibit EC migration (Fig. 1I), SEMA3A_A106K_ΔIg-b could not elicit an effective retraction of cultured ECs (fig. S10), similar to affinity-purified Fc-tagged SEMA3A_ΔIg-b. On the other hand, SEMA3A_WT was fully functional in this assay (Fig. 1C).

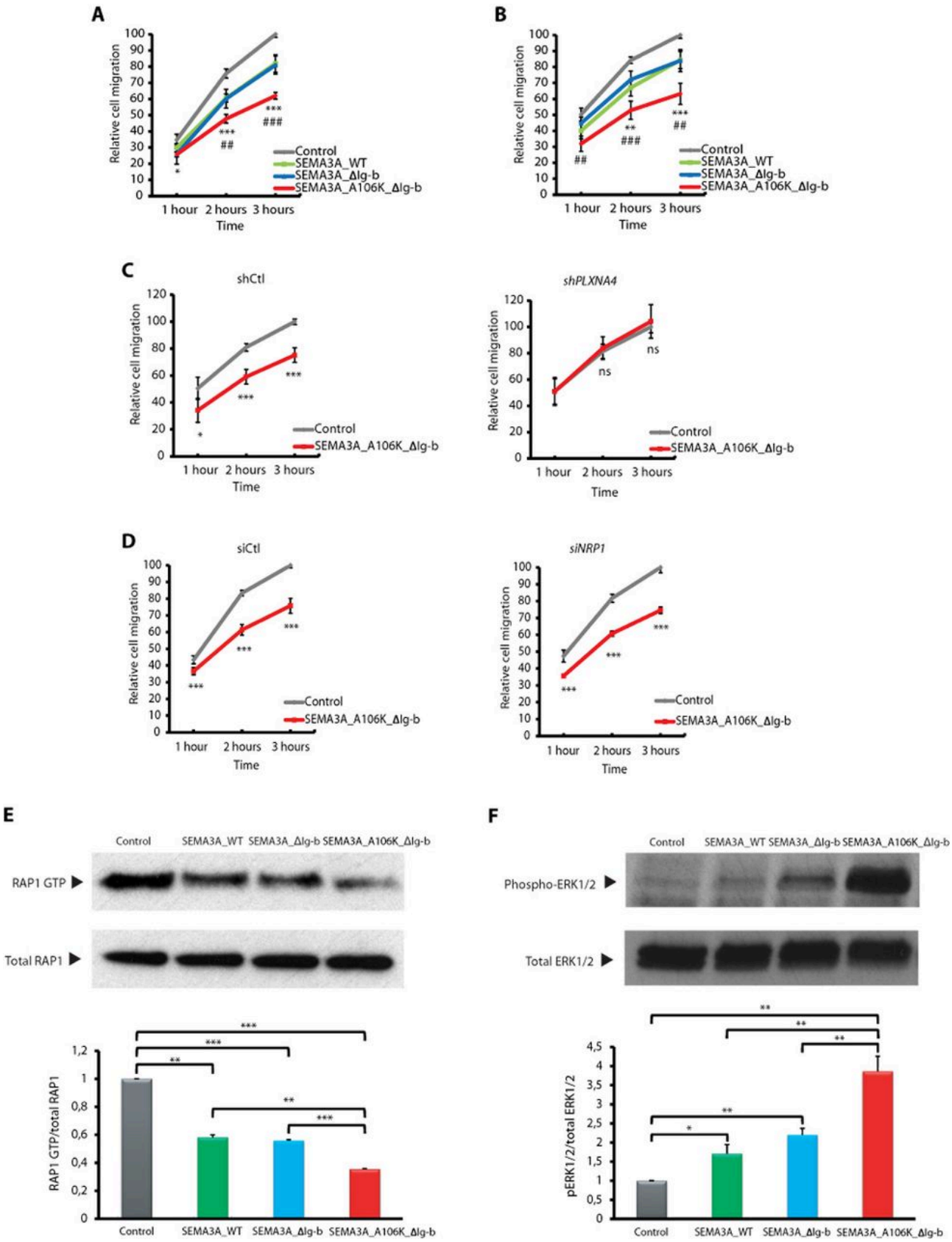

Fig. 5SEMA3A_A106K_**Δ**Ig-b is more effective than SEMA3A_WT and SEMA3A_**Δ**Ig-b in inhibiting directional migration and eliciting biochemical signaling in ECs.

(A and B) Real-time analysis of haptotactic EC migration toward Coll I either in the absence (control, gray) or in the presence of 0.9 nM (A) or 3.5 nM (B) recombinant SEMA3A_WT (green), SEMA3A_ΔIg-b (blue), or SEMA3A_A106K_ΔIg-b protein (red) was performed with an xCELLigence system. Results are the mean ± SEM of three independent experiments, with each experimental

point having been performed in triplicate. *SEMA3A_A106K_ΔIg-b versus SEMA3A_WT; #, SEMA3A_A106K_ΔIg-b versus SEMA3A_ΔIg-b. (C and D) Haptotactic migration toward Coll I of control (shCtl or siCtl), PLXNA4 (shPLXNA4)–silenced (C), or NRP1(siNRP1)–silenced (D) ECs was analyzed over time either in the absence (control, gray) or in the presence (red) of 1.8 nM SEMA3A_A106K_ΔIg-b protein. For simplicity, data from the same experiments are plotted in two separate graphs: shCtl (C) or siCtl (D) (left graph) and shPLXNA4 (C) or siNRP1 (D) (right graph). Results are the mean ± SEM of three (C) or four (D) independent experiments, with each experimental point having been performed in triplicate. (E) Pull-down assay of active RAP1 GTP in ECs that were treated or not for 1 min with 0.02 nM SEMA3A_WT, SEMA3A_ΔIg-b, or SEMA3A_A106K_ΔIg-b protein. For each experimental point, total RAP1, detected in the input fraction, was used to calculate the normalized amount of active RAP1 (RAP1 GTP/total RAP1). Results are the mean ± SEM of three independent biological replicates, one of which is shown. (F) Western blot analysis of activated phospho-ERK1/2 in ECs that were treated or not for 15 min with 0.2 nM SEMA3A_WT, SEMA3A_ΔIg-b, or SEMA3A_A106K_ΔIg-b protein. Western blot analysis of total ERK1/2 was used to calculate the normalized amount of active ERK1/2 (pERK1/2/total ERK1/2). Results are the mean ± SEM of four independent biological replicates, one of which is shown. Statistical analysis results were analyzed by a two-tailed heteroscedastic Student's t test; *P < 0.05, **/##P < 0.01, and ***/###P < 0.001.

All SEMAs signal through PLXN receptors, characterized by a cytosolic GAP activity (7) that inhibits small GTPases known for their ability to promote integrin-mediated cell adhesion to ECM proteins, including RAP1 (50, 51). In addition, similar to SEMA3E (52), but unlike SEMA3F (53, 54), SEMA3A was consistently reported to elicit the activation and phosphorylation of extracellular signal–regulated kinases 1 and 2 (ERK1/2) (55–59), which, in turn, induce the rapid synthesis of proteins that promote actin disassembly (60). We observed that Fc-tagged SEMA3A_A106K_ΔIg-b was significantly more powerful than SEMA3A_ΔIg-b (P < 0.001) and SEMA3A_WT (P < 0.01) in inhibiting the guanosine triphosphate (GTP) loading of RAP1 small GTPase (Fig. 5E), as evaluated in pull-down assays on purified glutathione S-transferase–Ral guanine nucleotide dissociation stimulator RAP1-binding domain, as well as in triggering the phosphorylation of ERK1/2 kinase in ECs (Fig. 5F). In addition, SEMA3A_A106K_ΔIg-b could elicit both signaling pathways independently of NRP1 expression in ECs (fig. S11). Therefore, we conclude that SEMA3A_A106K_ΔIg-b is an NRP1-independent, furin-resistant, stably dimeric, high-affinity PLXNA4 ligand capable of activating PLXN signaling and inhibiting EC haptotaxis much more powerfully than SEMA3A_WT.

SEMA3A_A106K_ΔIg-b protein is a parenterally deliverable inhibitor of cancer growth and metastatic dissemination

To assess whether the enhanced receptor binding, signaling, and biological activities in vitro, achieved by mutating A106 into K in the sema domain of SEMA3A, may also result in a greater therapeutic efficacy in vivo, independent of NRP1 involvement, we initially compared the antitumor properties of SEMA3A_ΔIg-b and SEMA3A_A106K_ΔIg-b in the RIP-Tag2 PNET mouse model. Consistently with in vitro data, we observed that AAV8-SEMA3A_A106K_ΔIg-b was 2.2-fold more effective than AAV8-SEMA3A_ΔIg-b in decreasing tumor burden in RIP-Tag2 mice (fig. S12A). These findings indicate that, likely due to its high-affinity binding to PLXNA4 and signaling strength, SEMA3A_A106K_ΔIg-b displays much greater anticancer efficacy than SEMA3A_ΔIg-b. On the basis of these data, we started to test the antitumoral properties of a purified SEMA3A_A106K_ΔIg-b recombinant protein in RIP-Tag2 mice. Notably, systemic administration of the minimal efficacious dose of SEMA3A_A106K_ΔIg-b protein in RIP-Tag mice (3 mg/kg, intraperitoneally, three times per week) hampered tumor growth by 67%, compared to controls (Fig. 6A). In addition, SEMA3A_A106K_ΔIg-b protein considerably reduced the volume of peripancreatic lymph node metastasis (Fig. 6, B and C).

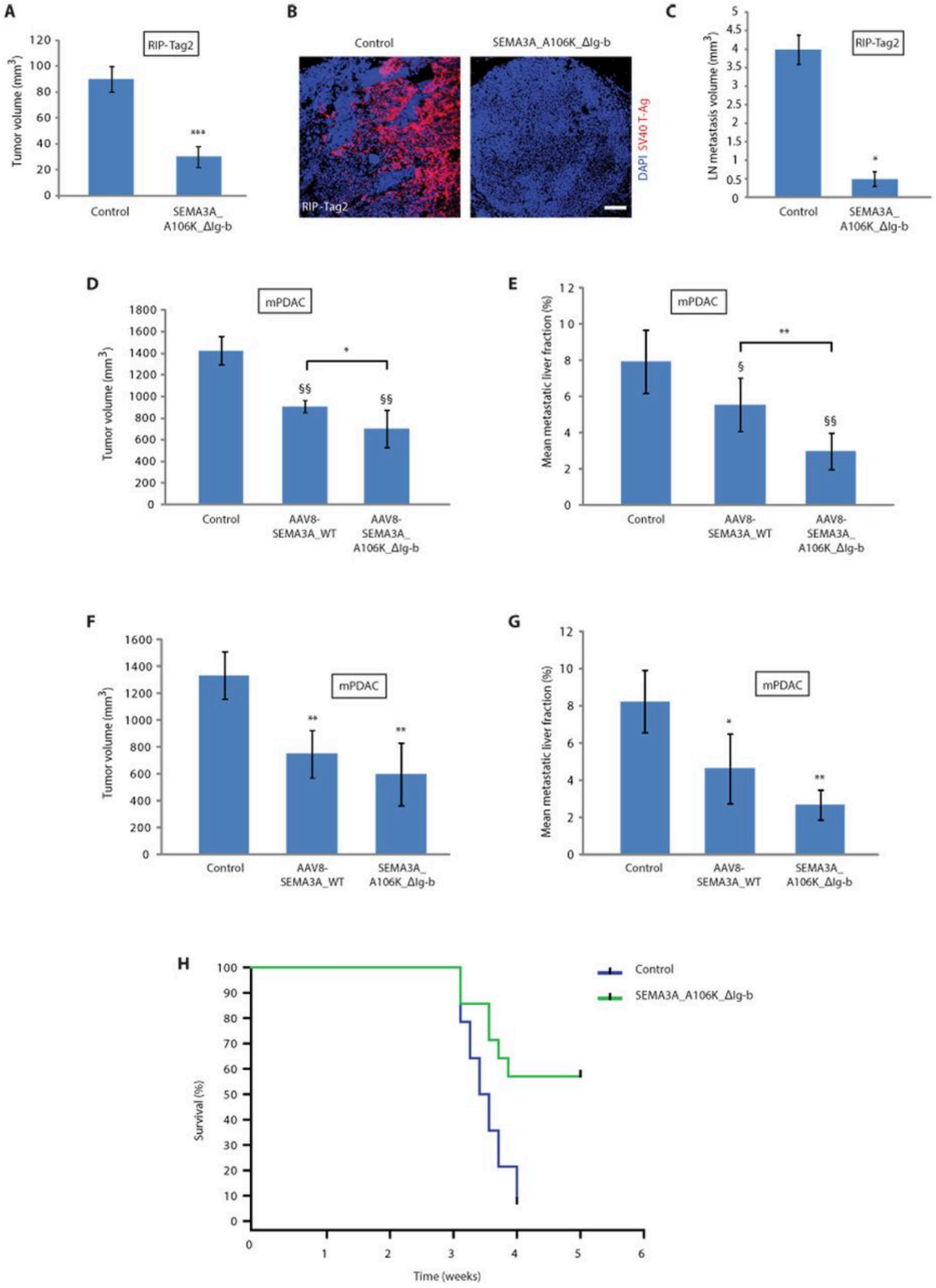

Fig. 6SEMA3A_A106K_**Δ**Ig-b inhibits tumor growth and metastatic dissemination in RIP-Tag2 and mPDAC models.

(A) Tumor volume of RIP-Tag2 mice treated with SEMA3A_A106K_ΔIg-b protein or control. (B) Confocal analysis of peripancreatic lymph node (LN) metastases, assessed by SV40 T-antigen (T-Ag) immunofluorescence (red); nuclei were counterstained with 4',6-diamidino-2-phenylindole (DAPI) (blue). Scale bar, 50 μm. (C) Effect of treatment with SEMA3A_A106K_ΔIg-b protein or control on LN metastasis volume (n = 10 per group). (D) Graphs show tumor volume of mPDAC mice treated for 3 weeks (n = 5 per group) with AAV8-SEMA3A_A106K_ΔIg-b or AAV8-SEMA3A_WT or control. §Treated sample versus control. (E) Total area of liver metastasis measured and plotted as metastatic liver fraction; §treated sample versus control. (F and G) Tumor volume (F) and liver metastasis area (G) of mPDAC treated for 3 weeks (n = 5 per group) with AAV8-SEMA3A_A106K_ΔIg-b or with SEMA3A_A106K_ΔIg-b. (H) Survival of tumor-bearing mPDAC mice continuously treated with SEMA3A_A106K_ΔIg-b protein or with saline buffer and sacrificed for ethical reasons at a prespecified clinical end point (n = 14 mice per group). Results are the mean ± SD, and results were analyzed by nonparametric two-tailed, unpaired Mann-Whitney U test; */§P < 0.05, **/§§P < 0.01, and ***P < 0.001; Kaplan-Meier survival curves were analyzed by Mantel-Cox test, **P < 0.01.

To further explore the therapeutic potential of SEMA3A_A106K_ΔIg-b, we investigated its effects in an orthotopic mouse model of the particularly aggressive histotype of PDAC (mPDAC), obtained by transplanting $Kras^{LSL\_G12D}$, $p53^{R172H/+}$, and $Ink4a/Arf^{flox/+}$ PDAC cells into the pancreas of syngeneic FVB/N mice. The mPDAC model recapitulates many features of human PDAC tumor cells and microenvironment, as we previously described (61). We initially treated mPDAC with AAV8-SEMA3A_WT or with AAV8-SEMA3A_A106K_ΔIg-b and assessed their effects on tumor volume and liver metastases. We observed that AAV8-SEMA3A_A106K_ΔIg-b displayed even greater antitumor effects than AAV8-SEMA3A_WT (51% versus 22% reduction of tumor volume compared to control, respectively; Fig. 6D). More pronounced was the effect of treatment on liver metastasis. Metastasis area was effectively reduced in AAV8-SEMA3A_A106K_ΔIg-b–transduced mice compared to both control- and AAV8-SEMA3A_WT–treated mPDAC animals (by 62 and 46%, respectively) (Fig. 6E). Then, in the same experimental setting, we validated the therapeutic efficacy of the recombinant purified SEMA3A_A106K_ΔIg-b protein and observed that total tumor burden and metastasis area were decreased both in mice treated with AAV8-SEMA3A_A106K_ΔIg-b and in those treated with SEMA3A_A106K_ΔIg-b recombinant protein (by 43 and 55% for tumor volume and by 44 and 68% for liver metastases, respectively) (Fig. 6, F and G). In addition, in a side-by-side comparison, SEMA3A_A106K_ΔIg-b protein displayed a greater antitumor activity than SEMA3A_ΔIg-b (fig. S12, B and C). Thus, SEMA3A_A106K_ΔIg-b, either delivered by gene transfer or parenterally administered as a recombinant protein, efficiently hampers mPDAC growth and metastatic dissemination. In this experimental setting, the impact of SEMA3A_A106K_ΔIg-b protein on pancreatic tumor volume can only be assessed at the end of the experiment when the mice are sacrificed. To monitor the kinetics of the therapeutic effect, we treated different cohorts of mPDAC mice for 1, 2, or 3 weeks only. We started the therapy 1 week after the injection of PDAC cells into the pancreas and measured the tumor burden in randomly selected mice sacrificed after 1, 2, or 3 weeks of continued treatment. We observed that parenterally delivered recombinant SEMA3A_A106K_ΔIg-b (3 mg/kg, three times per week) inhibited tumor growth, resulting in a significant (P < 0.01) cumulative effect after 3 weeks of treatment, when the experiment was terminated for ethical reasons, due to the excessive growth of untreated tumors in control mice (fig. S13).

Then, we assessed whether the observed antitumor effects of SEMA3A_A106K_ΔIg-b protein would also enhance the survival of mPDAC mice, which, as we previously described (61), typically die between the third and fourth week after cancer cell injection into the pancreas, due to both primary tumor burden and liver metastases. We set up a survival trial in which we predefined a clinical end point at which the mice were sacrificed due to signs of serious sickness, indicating forthcoming death, and periodically assessed the survival of mice for up to 5 weeks after tumor injection. As expected, all control-treated mPDAC animals died or had to be sacrificed between the third and fourth week. By contrast, 8 of 14 SEMA3A_A106K_ΔIg-b–treated mice survived for at least 5 weeks, until the end of the experiment, when they were sacrificed. Together, these findings provide evidence that parenteral delivery of SEMA3A_A106K_ΔIg-b protein hampers tumor growth, impairs metastatic dissemination, and prolongs survival by 57% (*P < 0.05) (Fig. 6H).

Finally, a 3-week treatment with SEMA3A_A106K_ΔIg-b protein at different dosing regimens did not elicit any detectable signs of toxicity in mice in terms of body weight changes, abnormalities in kidney or liver function, or blood counts (fig. S14 and tables S2 and S3). Moreover, rotarod performance tests showed that SEMA3A_A106K_ΔIg-b protein did not

alter motor function in mice (fig. S15). Together, these findings provide evidence that NRP1-independent SEMA3A_A106K_ΔIg-b is an effective, nontoxic, parenterally deliverable anticancer agent.

SEMA3A_A106K_ΔIg-b normalizes the tumor vasculature and enhances the anticancer potential of chemotherapeutic drugs

We previously demonstrated that AAV8-delivered SEMA3A_WT normalizes the cancer vasculature and strongly reduces the hypoxia-driven transcription of prometastatic genes (11, 13). Thus, we assessed the vascular normalizing activity of recombinant SEMA3A_A106K_ΔIg-b protein in both RIP-Tag2 and mPDAC models. One month of treatment of RIP-Tag2 mice with SEMA3A_A106K_ΔIg-b protein reduced tumor blood vessel area by 51% (Fig. 7A), increased pericyte coverage by 40% (Fig. 7B), and enhanced vascular perfusion by 77% (Fig. 7C). In line with the increased pericyte coverage and perfusion of tumor blood vessels (Fig. 7, B and C), we also observed a significant (79%; $P < 0.001$) reduction of tumor hypoxia in SEMA3A_A106K_ΔIg-b protein–treated mice compared to controls (Fig. 7D). A 3-week administration of SEMA3A_A106K_ΔIg-b protein also effectively induced vascular normalization and increased blood vessel pericyte coverage by 78% in mPDAC tumors (Fig. 7E). In addition, we found that blood vessel perfusion was increased by 85% (Fig. 7F), and tumor hypoxia was reduced by 81% (Fig. 7G) in SEMA3A_A106K_ΔIg-b protein–treated mPDAC animals compared to controls.

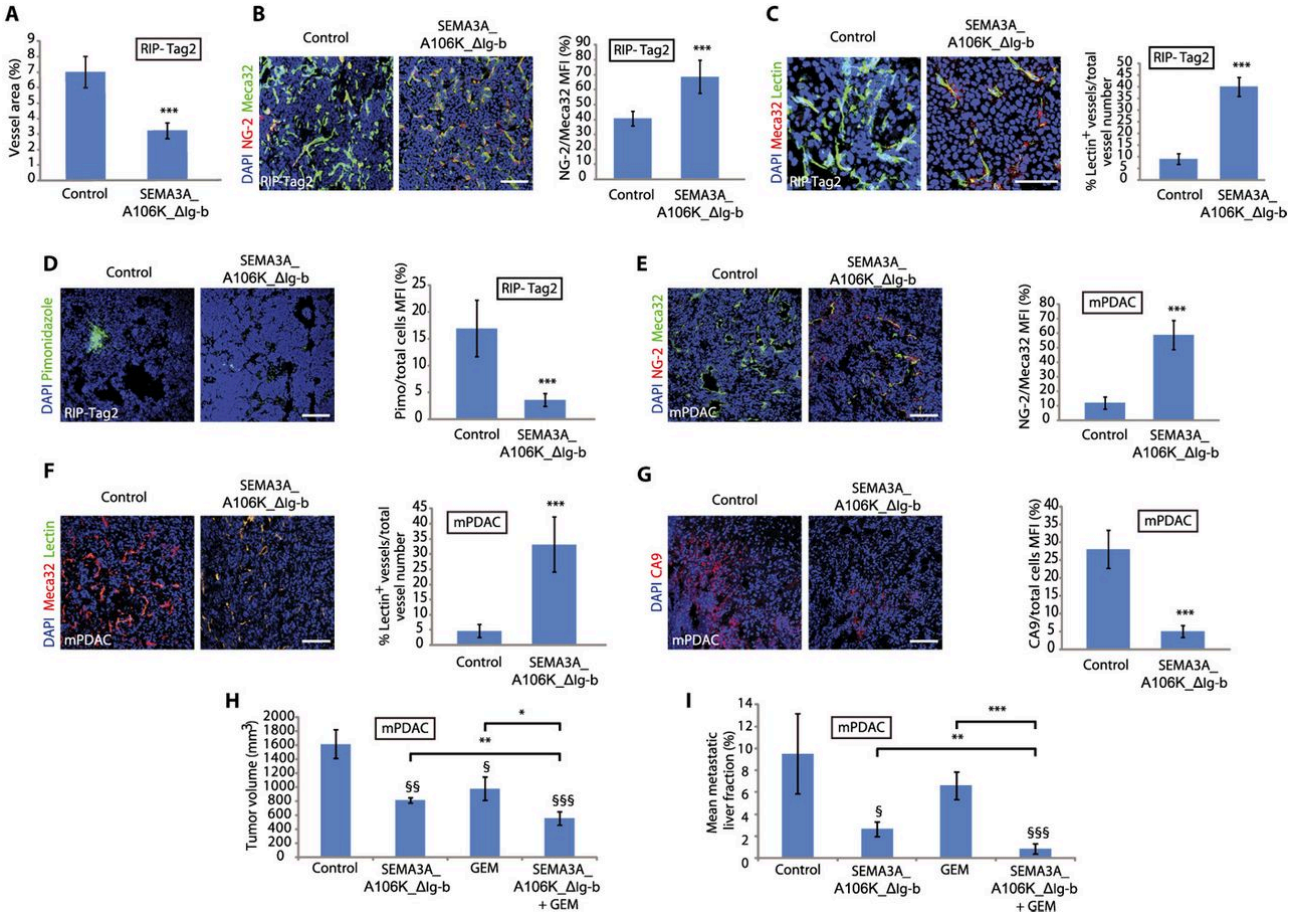

Fig. 7SEMA3A_A106K_ΔIg-b normalizes the vasculature of RIP-Tag2 and mPDAC mice and sensitizes PDAC tumors to GEM.

(A) Confocal analysis of Meca32 immunostaining evaluating vessel density in SEMA3A_A106K_ΔIg-b protein–treated RIP-Tag2 tumors and controls. (B) In RIP-Tag2 mice, blood vessel pericyte coverage after treatment with control or SEMA3A_A106K_ΔIg-b protein was evaluated by colocalization of Meca32 (green) and NG-2 (red). (C) Blood vessel perfusion was evaluated by lectin (green) colocalization with Meca32 (red) in RIP-Tag2 tumors. (D) Tumor hypoxia was assessed by pimonidazole adduct immunostaining in SEMA3A_A106K_ΔIg-b protein–treated RIP-Tag2 tumors and controls. (E) Confocal analysis revealed pericyte coverage in blood vessels of SEMA3A_A106K_ΔIg-b protein–treated PDAC mice and controls, as assessed by colocalization of

Meca32 (green) and NG-2 (red). (F) Lectin (green) colocalized with Meca32 (red) showed vessel perfusion in mPDAC treated with SEMA3A_A106K_ΔIg-b protein and controls. (G) Tumor hypoxia was assessed in mPDAC after treatment with SEMA3A_A106K_ΔIg-b or control by immunostaining with carbonic anhydrase (CA9) antibody. Results are from five fields per mouse (n = 5 per treatment group). (H and I) mPDAC mice were treated for 3 weeks with the following: (i) SEMA3A_A106K_ΔIg-b protein (3 mg/kg, intraperitoneally, three times per week), (ii) GEM (50 mg/kg, intravenously, twice per week), (iii) SEMA3A_A106K_ΔIg-b protein + GEM, and (iv) control (saline solution) (n = 11 per group). (H) Analysis of tumor volume; the combination of the two drugs (SEMA3A_A106K_ΔIg-b + GEM) more efficiently reduced tumor burden (by 66%) compared with the vehicle-treatment group. §Treated sample versus control. (I) Analysis of the total area of liver metastasis; SEMA3A_A106K_ΔIg-b + GEM more effectively impaired the liver metastasis fraction compared to single drugs (by 90, 87, and 67% compared with controls, GEM, or SEMA3A_A106K_ΔIg-b alone, respectively). §Treated sample versus control. Results are the mean ± SD and were analyzed by nonparametric two-tailed, unpaired Mann-Whitney U test; */§P < 0.05, **/§§P < 0.01, and ***/§§§P < 0.001. Scale bars, 50 μm.

To evaluate whether SEMA3A_A106K_ΔIg-b–elicited tumor blood vessel normalization may improve the delivery and the anticancer activity of chemotherapeutic drugs, we next treated cohorts of PDAC mice with SEMA3A_A106K_ΔIg-b protein alone, gemcitabine (GEM) alone, or the combination of both molecules (SEMA3A_A106K_ΔIg-b + GEM). The coadministration of SEMA3A_A106K_ΔIg-b protein with GEM was more efficient at inhibiting tumor growth (Fig. 7H) and metastatic spread to the liver (Fig. 7I) than the corresponding drugs used as single agents. In addition, SEMA3A_A106K_ΔIg-b protein, as a single agent, displayed a stronger antimetastatic activity than GEM alone (Fig. 7I). These data provide evidence that SEMA3A_A106K_ΔIg-b protein is a vessel-normalizing drug that efficiently enhances the delivery and the anticancer properties of GEM in PDACs.

SEMA3A_A106K_ΔIg-b decreases laser-induced choroidal neovascularization of the retina

In addition to cancer, another relevant example of pathological angiogenesis in humans is choroidal neovascularization (CNV) of the retina that is typical of the exudative form of age-related macular degeneration (AMD), a leading cause of vision loss worldwide (62). We compared the effect of intraocular delivery of different amounts (1, 10, or 100 ng/ml) of recombinant SEMA3A_WT or SEMA3A_A106K_ΔIg-b protein in the laser-induced CNV mouse model, which faithfully recapitulates human exudative AMD (63). We observed that although intraocular delivery of recombinant SEMA3A_WT (1 or 10 ng/ml) did not affect laser-induced CNV, the same amounts of SEMA3A_A106K_ΔIg-b protein inhibited CNV by 22% (1 ng/ml) or 30% (10 ng/ml) (fig. S16). Injection of larger quantities (100 ng/ml) of either SEMA3A_WT or SEMA3A_A106K_ΔIg-b recombinant proteins had similar effects on CNV (fig. S16).

DISCUSSION

Growing clinical evidence indicates how improving cancer perfusion and oxygenation by means of vascular normalization may allow patients to survive longer due to reduced invasion of distant organs and enhanced therapeutic outcome (1). We previously described AAV-conveyed SEMA3A_WT as an effective vascular normalizing and anticancer agent in mouse preclinical models (11–13). However, SEMA3A_WT was also reported to trigger adverse (21, 22) and protumoral (20) side effects via NRP1, which, along with PLXNAs, is usually considered to be an essential SEMA3A_WT holoreceptor component (7). Here, we describe the generation and characterization of a parenterally deliverable, NRP1-independent, and therapeutically safe SEMA3A_A106K_ΔIg-b mutant protein isoform that, owing to its ability to bind PLXNA4 with high affinity, efficiently normalizes the cancer vasculature and impairs metastatic progression.

In contrast to the current widely accepted model of SEMA3A signaling (7, 8), we provide evidence that NRP1 is essential for some, but not all, SEMA3A functions both in vitro and in vivo. We show how SEMA3A chemorepels EC migration, promotes vascular normalization, and inhibits cancer growth and metastatic dissemination independently from its high-affinity binding to NRP1. The latter is mediated by the basic C-terminal stretch of SEMA3A_WT protein that is needed to prompt active $\alpha_5\beta_1$ integrin endocytosis, EC collapse, and blood vessel permeability. It is thus possible that SEMA3A_WT elicits NRP1-dependent EC contraction and vascular leakage by promoting the endocytosis of adhesion

receptors, such as integrins. Our results are consistent with previous observations that NRP1 drives active $\alpha_5\beta_1$ integrin endocytosis (33) and that C-end rule peptide binding to NRP1 b1 domain fosters macropinocytosis (30, 36, 64) and vascular leakage (30). Furthermore, SEMA3A_WT also repels neuron growth cones by stimulating massive macropynocitosis and NRP1 endocytosis (65–67).

Notably, the NRP1-independent SEMA3A_ΔIg-b mutant protein allowed us to clarify why NRP1 is fully dispensable for SEMA3A inhibition of RAP1 GTP loading and haptotactic migration of ECs. Because it does not bind PLXNA4 with high affinity, SEMA3A_ΔIg-b likely connects on the EC surface to co-receptors other than NRP1. In this respect, plausible candidates may be chondroitin sulfate proteoglycans that, in addition to controlling angiogenesis (68), bind and promote SEMA3A inhibitory activity on the outgrowth of neurites from dorsal root ganglia (69). Moreover, our findings are in accordance with previous in vivo analyses of PlxnA4 knockout mice, hinting that in vivo SEMA3A might control some axon projections through PLXNA4 signaling but independently from NRP1 (34). Our findings show that SEMA3A can trigger two distinct and parallel pathways, via PLXNA4 and via the NRP1 receptor. It is conceivable that the emergence of neuropilins in vertebrates (70) may have bolstered the coevolution of SEMA3 proteins that, compared to other family members, appear to have more complex and combinatorial forward-signaling properties.

On the therapeutic side, we observed that, contrary to what was previously assumed (7), the interaction with NRP1 is functionally dispensable for SEMA3A to inhibit cancer progression. In this regard, preventing binding to a major co-receptor, such as NRP1, could substantially decrease the antitumor activity of SEMA3A, even if it helps overcome adverse effects (20, 21). However, our rationally designed mutagenesis approach demonstrated that electrostatic charges within the extrusion 1 region of the sema domain are crucial regulators of SEMA3A binding to PLXNA4 and activation of downstream signals. Thus, the introduction of a single positively charged amino acid (A106K) in extrusion 1 was sufficient to markedly increase the affinity of SEMA3A for PLXNA4 along with the strength of its biochemical and biological activities, both on vascular ECs and in preclinical models of pancreatic cancer.

A major clinical benefit of tumor blood vessel normalization is the possibility of enhancing delivery of anticancer drugs and, thus, their efficacy (1). In the case of PDAC patients, the combination of targeted agents and chemotherapy did not extend survival, and available antiangiogenic agents failed to improve the reduced supply of drugs that is typical of PDAC (71). Herein, we showed that SEMA3A_A106K_ΔIg-b protein considerably prolongs the survival of mPDAC mice. Moreover, by enhancing the anticancer properties of the standard-of-care GEM, SEMA3A_A106K_ΔIg-b protein efficiently inhibited tumor growth and hindered metastatic dissemination of PDAC to the liver. SEMA3A_A106K_ΔIg-b protein was therapeutically more effective than recombinant SEMA3A_WT, further demonstrating that A106K mutation endows this protein with enhanced anticancer properties. Similarly, low amounts of SEMA3A_A106K_ΔIg-b, but not of SEMA3A_WT, inhibited retinal CNV in mice, a well-accepted model of the human form of exudative AMD. The molecular dynamics–aided insertion of charged amino acid(s) in strategic positions of the extrusion 1 of other SEMA3 proteins, such as SEMA3B, may similarly increase their binding to cognate PLXN receptors and allow the generation of effective and therapeutically exploitable SEMA3 mutants.

Here, we evaluated the antitumor properties of the NRP1-independent superagonist SEMA3A_A106K_ΔIg-b mutant in two different pancreatic cancer histotypes, namely, exocrine ductal adenocarcinoma and neuroendocrine insulinoma. It should be noted that the therapeutic efficacy of SEMA3A_A106K_ΔIg-b could vary among diverse cancer types, for instance, due to differences in the tumor microenvironment (TME). Thus, further assessment of the activity of SEMA3A_A106K_ΔIg-b in additional cancer types will be needed, ideally focusing on those in which TME and vascular abnormalities, tissue hypoxia, and aberrantly activated stromal cells play a prominent role in tumor growth and metastatic progression.

In summary, we show that SEMA3A may act independently from NRP1 and identify a key point mutation (A106K) that allows high-affinity binding to PLXNA4, the major SEMA3A signaling receptor in neurons (34) and ECs (35). The mutated SEMA3A_A106K_ΔIg-b non-natural protein isoform should provide a powerful, safe, and clinically exploitable vascular normalizing agent in cancer and other diseases characterized by pathological angiogenesis, such as retinal AMD.

MATERIALS AND METHODS

Study design

This study was aimed to rationally design a mutant version of SEMA3A capable of exerting its biological activity in an NRP1-independent manner. We first generated SEMA3A_ΔIg-b, a SEMA3A deletion mutant that can no longer bind NRP1, and then characterized its biological activities in vitro and in vivo. Next, because the lack of NRP1 binding caused a substantial change in the functional properties of SEMA3A_ΔIg-b compared to the wild-type molecule, we sought to increase its affinity for PLXNA receptors through a point mutation. To this end, we designed and produced a mutated SEMA3A_A106K_ΔIg-b and then characterized its ability to interact with different PLXNAs (alone or in combination with NRP1), establishing that the SEMA3A_A106K_ΔIg-b selectively binds PLXNA4 with high affinity. Subsequently, we characterized the biological activities of SEMA3A_A106K_ΔIg-b in vitro. All in vitro results are representative of two to six independent experiments. To evaluate the efficacy of SEMA3A_A106K_ΔIg-b in inhibiting tumor growth and metastatic dissemination, we performed preclinical trials treating spontaneous PNET of RIP-Tag2 mice and an orthotopic mouse model of mPDAC. We treated cohorts of either model with SEMA3A_WT, SEMA3A_ΔIg-b, SEMA3A_A106K_ΔIg-b, or saline solution and compared tumor growth and metastasis. In addition, we treated a cohort of mPDAC mice with SEMA3A_A106K_ΔIg-b or saline solution and assessed the effect on mouse survival. Data were analyzed by a Kaplan-Meier curve and the Mantel-Cox test. In animal studies, mice were randomized 1 week after injection of tumor cells, when tumors were established, to ensure similar tumor sizes in all treatment groups. The primary end points were survival along with the size of the primary tumor and metastases. For each experiment, mouse numbers and statistical tests are described in the figure legends and in Supplementary Materials and Methods. To evaluate the mechanisms behind the therapeutic effects of SEMA3A_A106K_ΔIg-b, we analyzed the vasculature of tumors derived from RIP-Tag2 and mPDAC mice in the different treatment groups by checking several markers of vessel normalization. To further investigate the normalizing effect of SEMA3A_A106K_ΔIg-b and its ability to improve the delivery and efficacy of chemotherapeutic drugs in pancreatic cancer, we treated mPDAC mice with SEMA3A_A106K_ΔIg-b in combination with GEM and compared their effect on tumor growth and metastasis. All procedures were performed in accordance with institutional protocols approved by the Ethics Committee of the University of Torino and by the Italian Ministry of Health in compliance with international laws and policies.

Statistics

Results of the experiments are expressed as mean ± SD or SEM. Parametric two-tailed heteroscedastic Student's t test was used to assess the statistical significance when two groups of unpaired normally distributed values were compared; when more than two groups were compared, parametric two-tailed analysis of variance (ANOVA) with Bonferroni's post hoc analysis was applied. Nonparametric two-tailed Mann-Whitney U test was used to calculate the statistical significance when two groups of unpaired and not normally distributed values were compared. Nonparametric Mantel-Cox test was performed to evaluate the statistical significance of the distribution over time of a nominal variable, such as survival, between two samples. $P < 0.05$ was considered significant. Original data are provided in table S4.

SUPPLEMENTARY MATERIALS

www.sciencetranslationalmedicine.org/cgi/content/full/10/442/eaah4807/DC1

Materials and Methods

Fig. S1. Purification of Fc-tagged SEMA3A_ΔIg-b and SEMA3A_A106K_ΔIg-b recombinant proteins.

Fig. S2. SEMA3A_ΔIg-b protein effect on tumor growth in RIP-Tag2 mice.

Fig. S3. SEMA6A-PLXNA2 and SEMA3A$_{A106K}$-PLXNA4 interaction details.

Fig. S4. Structural comparison of key residues involved in the charge complementarity of the extrusion region.

Fig. S5. Root mean square deviation of the backbone atoms from the starting SEMA6A-PLXNA2 and SEMA3A$_{A106K}$-PLXNA4 structures as a function of time.

REFERENCES AND NOTES

1. R. K. Jain, Antiangiogenesis strategies revisited: From starving tumors to alleviating hypoxia. Cancer Cell 26, 605–622 (2014).

2. S. M. Welford, A. J. Giaccia, Hypoxia and senescence: The impact of oxygenation on tumor suppression.Mol. Cancer Res. 9, 538–544 (2011).

3. G. L. Semenza, Dynamic regulation of stem cell specification and maintenance by hypoxia-inducible factors. Mol. Aspects Med. 47–48, 15–23 (2016).

4. A. Casazza, G. Di Conza, M. Wenes, V. Finisguerra, S. Deschoemaeker, M. Mazzone, Tumor stroma: A complexity dictated by the hypoxic tumor microenvironment. Oncogene 33, 1743–1754 (2014).

5. D. M. Gilkes, G. L. Semenza, D. Wirtz, Hypoxia and the extracellular matrix: Drivers of tumour metastasis.Nat. Rev. Cancer 14, 430–439 (2014).

6. M. Greaves, Evolutionary determinants of cancer. Cancer Discov. 5, 806–820 (2015).

7. T. Worzfeld, S. Offermanns, Semaphorins and plexins as therapeutic targets.Nat. Rev. Drug Discov. 13,603–621 (2014).

8. A. Kumanogoh, H. Kikutani, Immunological functions of the neuropilins and plexins as receptors for semaphorins. Nat. Rev. Immunol. 13, 802–814 (2013).

9. L. Tamagnone, Emerging role of semaphorins as major regulatory signals and potential therapeutic targets in cancer. Cancer Cell 22, 145–152 (2012).

10.G. Serini, D. Valdembri, S. Zanivan, G. Morterra, C. Burkhardt, F. Caccavari, L. Zammataro, L. Primo, L.Tamagnone, M. Logan, M. Tessier-Lavigne, M. Taniguchi, A. W. Püschel, F. Bussolino, Class 3 semaphorins control vascular morphogenesis by inhibiting integrin function. Nature 424, 391–397 (2003).

11. G. Serini, F. Bussolino, F. Maione, E. Giraudo, Class 3 semaphorins: Physiological vascular normalizing agents for anti-cancer therapy. J. Intern. Med. 273, 138–155 (2013).

12.F. Maione, F. Molla, C. Meda, R. Latini, L. Zentilin, M. Giacca, G. Seano, G. Serini, F. Bussolino, E. Giraudo ,Semaphorin 3A is an endogenous angiogenesis inhibitor that blocks tumor growth and normalizes tumor vasculature in transgenic mouse models. J. Clin. Invest. 119, 3356–3372 (2009).

13.F. Maione, S. Capano, D. Regano, L. Zentilin, M. Giacca, O. Casanovas, F. Bussolino, G. Serini, E. Giraudo, Semaphorin 3A overcomes cancer hypoxia and metastatic dissemination induced by antiangiogenic treatment in mice. J. Clin. Invest. 122, 1832–1848 (2012).

14. C. Tang, X. Gao, H. Liu, T. Jiang, X. Zhai, Decreased expression of SEMA3A is associated with poor prognosis in gastric carcinoma. Int. J. Clin. Exp. Pathol. 7, 4782–4794 (2014).

15.L. Yan-Chun, Y. Hong-Mei; C. Zhi-Hong; H. Qing; Z. Yan-Hong; W. Ji-Fang, MicroRNA-192-5p promote the proliferation and metastasis of hepatocellular carcinoma cell by targeting SEMA3A. Appl. Immunohistochem. Mol. Morphol. 25, 251–260 (2015).

16.M. Yacoub, A. Coulon, O. Celhay, J. Irani, O. Cussenot, G. Fromont, Differential expression of the semaphorin 3A pathway in prostatic cancer. Histopathology 55, 392–398 (2009).

17. X. Song, W. Zhang, Y. Zhang, H. Zhang, Z. Fu, J. Ye, L. Liu, X. Song, Y. Wu, Expression of semaphorin 3A and neuropilin 1 with clinicopathological features and survival in human tongue cancer. Med. Oral Patol. Oral Cir. Bucal 17, e962–e968 (2012).

18. V. Barresi, E. Vitarelli, S. Cerasoli, Semaphorin3A immunohistochemical expression in human meningiomas: Correlation with the microvessel density. Virchows Arch. 454, 563–571 (2009).

19. P. J. Bailey, D. K. Chang, K. Nones, A. L. Johns, A.-M. Patch, M.-C. Gingras, D. K. Miller, A. N. Christ, T. J. C. Bruxner, M.C. Quinn, C. Nourse, L.C. Murtaugh, I. Harliwong, S. Idrisoglu, S. Manning, E. Nourbakhsh, S.Wani, L. Fin k, O. Holmes, V. Chin, M.J. Anderson, S. Kazakoff, C. Leonard, F. Newell, N. Waddell, S. Wood, Q.Xu, P.J. Wilson, N. C loonan, K.S. Kassahn, D. Taylor, K. Quek, A.J. Robertson, L. Pantano, L. Mincarelli, L.N. Sánchez, L.M. Evers, J. Wu, M . Pinese, M.J. Cowley, M.D. Jones, E.K. Colvin, A.M. Nagrial, E.S.Humphrey, L.A. Chantrill, A. Mawson, J. Humphris, A. Chou, M. Pajic, C. J. Scarlett, A. V. Pinho, M. Giry-Laterriere, I. Rooman, J. S. Samra, J. G. Kench, J. A. Lovell, N. D. Merrett, C.W. Toon, K. Epari, N.Q. Nguyen,A. Barbour, N. Zeps, K. MoranJones, N.B. Jamieson, J.S. Graham, F. Dut hie, K. A. Oien, J. Hair, R.Grützmann, A. Maitra, C. A. Iacobuzio-Donahue, C. L. Wolfgang, R. A. Morgan, R. T. Lawlor, V. Corbo, C.Bassi, B. Rusev, P. Capelli, R. Salvia, G. Tortora, D. Mukhopadhyay, G. M. Petersen Australian Pancreatic Cancer Genome Initiative, D. M. Munzy, W. E. Fisher, S. A. Karim, J. R. Eshleman, R. H. Hruban, C. Pilarsky,J. P. Morton, O. J. Sansom, A. Scarpa, E. A. Musgrove, U.-M. H. Bailey, O. Hofmann, R. L. Sutherland, D. A.Wheeler, A. J. Gill, R. A. Gibbs, J. V. Pearson, N. Waddell, A. V. Biankin, S. M. Grimmond, Genomic analyses identify molecular subtypes of pancreatic cancer. Nature 531, 47–52 (2016).

20. A. Casazza, D. Laoui, M. Wenes, S. Rizzolio, N. Bassani, M. Mambretti, S. Deschoemaeker, J. A. Van Ginderachter, L. Tamagnone, M. Mazzone, Impeding macrophage entry into hypoxic tumor areas by Sema3A/NRP1 signaling blockade inhibits angiogenesis and restores antitumor immunity. Cancer Cell 24,695–709 (2013).

21. L. M. Acevedo, S. Barillas, S. M. Weis, J. R. Göthert, D. A. Cheresh, Semaphorin 3A suppresses VEGF-mediated angiogenesis yet acts as a vascular permeability factor. Blood 111, 2674–2680 (2008).

22.A. Cerani, N. Tetreault, C. Menard, E. Lapalme, C. Patel, N. Sitaras, F. Beaudoin, D. Leboeuf, V. De Guire, F.Binet, A. Dejda, F. A. Rezende, K. Miloudi, P. Sapieha, Neuron-derived semaphorin 3A is an early inducer of vascular permeability in diabetic retinopathy via neuropilin-1. Cell Metab. 18, 505–518 (2013).

23. C. Siebold, E. Y. Jones, Structural insights into semaphorins and their receptors. Semin. Cell Dev. Biol.24, 139–145 (2013).

24. A. Antipenko, J.-P. Himanen, K. van Leyen, V. Nardi-Dei, J. Lesniak, W. A. Barton, K. R. Rajashankar, M. Lu,C. Hoemme, A. W. Püschel, D. B. Nikolov, Structure of the semaphorin-3A receptor binding module. Neuron39, 589–598 (2003).

25. A. M. Koppel, J. A. Raper, Collapsin-1 covalently dimerizes, and dimerization is necessary for collapsing activity. J. Biol. Chem. 273, 15708–15713 (1998).

26. H.-F. Guo, C. W. Vander Kooi, Neuropilin functions as an essential cell surface receptor. J. Biol. Chem.290, 29120–29126 (2015).

27. B. J. C. Janssen, Tomas Malinauskas, G. A. Weir, M. Z. Cader, C. Siebold, E. Y. Jones, Neuropilins lock secreted semaphorins onto plexins in a ternary signaling complex. Nat. Struct. Mol. Biol. 19, 1293–1299(2012).

28.T. Nogi, N. Yasui, E. Mihara, Y. Matsunaga, M. Noda, N. Yamashita, T. Toyofuku, S. Uchiyama, Y. Goshima,A. Kum anogoh, J. Takagi, Structural basis for semaphorin signalling through the plexin receptor. Nature467, 1123–1127 (2010).

29. R. H. Adams, M. Lohrum, A. Klostermann, H. Betz, A. W. Püschel, The chemorepulsive activity of secreted semaphorins is regulated by furin-dependent proteolytic processing. EMBO J. 16, 6077–6086(1997).

30. T. Teesalu, K. N. Sugahara, V. R. Kotamraju, E. Ruoslahti, C-end rule peptides mediate neuropilin-1-dependent cell, vascular, and tissue penetration. Proc. Natl. Acad. Sci. U.S.A. 106, 16157–16162 (2009).

31.N. Guttmann-Raviv, N. Shraga-Heled, A. Varshavsky, Cinthya Guimaraes-Sternberg, O. Kessler, G.Neufeld, Semaphorin-3A and semaphorin-3F work together to repel endothelial cells and to inhibit their survival by induction of apoptosis. J. Biol. Chem. 282, 26294–26305 (2007).

32. C. Camillo, N. Gioelli, F. Bussolino, G. Serini, An electrical impedance-based method for quantitative real-time analysis of semaphorin-elicited endothelial cell collapse. Methods Mol. Biol. 1493, 195–207 (2017).

33. D. Valdembri, P. T. Caswell, K. I. Anderson, J. P. Schwarz, I. König, E. Astanina, F. Caccavari, J. C. Norman,M. J. Humphries, F. Bussolino, G. Serini, Neuropilin-1/GIPC1 signaling regulates α5β1 integrin traffic and function in endothelial cells. PLOS Biol. 7, e1000025 (2009).

34. A. Yaron, P. H. Huang, H. J. Cheng, M. Tessier-Lavigne, Differential requirement for Plexin-A3 and -A4 in mediating responses of sensory and sympathetic neurons to distinct class 3 Semaphorins. Neuron 45,513–523 (2005).

35. B. Kigel, N. Rabinowicz, A. Varshavsky, O. Kessler, G. Neufeld, Plexin-A4 promotes tumor progression and tumor angiogenesis by enhancement of VEGF and bFGF signaling. Blood 118, 4285–4296 (2011).

36. H.-B. Pang, G. B. Braun, E. Ruoslahti, Neuropilin-1 and heparan sulfate proteoglycans cooperate in cellular uptake of nanoparticles functionalized by cationic cell-penetrating peptides. Sci. Adv. 1, e1500821(2015).

37. A. Sakurai, J. Gavard, Y. Annas-Linhares, J. R. Basile, P. Amornphimoltham, T. R. Palmby, H. Yagi, F.Zhang, P. A. Randazzo, X. Li, R. Weigert, J. S. Gutkind, Semaphorin 3E initiates antiangiogenic signaling through plexin D1 by regulating Arf6 and R-Ras. Mol. Cell. Biol. 30, 3086–3098 (2010).

38. M. Radu, J. Chernoff, An in vivo assay to test blood vessel permeability. J. Vis. Exp. 73, e50062 (2013).

39. B. J. C. Janssen, R. A. Robinson, F. Pérez-Brangulí, C. H. Bell, K. J. Mitchell, C. Siebold, E. Y. Jones,Structural basis of semaphorin–plexin signalling. Nature 467, 1118–1122 (2010).

40. I. S. Moreira, P. A. Fernandes, M. J. Ramos, Hot spots—A review of the protein-protein interface determinant amino-acid residues. Proteins 68, 803–812 (2007).

41. U. Yazdani, J. R. Terman, The semaphorins. Genome Biol. 7, 211 (2006).

42. A. L. Kolodkin, D. V. Levengood, E. G. Rowe, Y.-T. Tai, R. J. Giger, D. D. Ginty, Neuropilin is a semaphorin III receptor. Cell 90, 753–762 (1997).

43. A. Varshavsky, O. Kessler, S. Abramovitch, B. Kigel, S. Zaffryar, G. Akiri, G. Neufeld, Semaphorin-3B is an angiogenesis inhibitor that is inactivated by furin-like pro-protein convertases. Cancer Res. 68, 6922–6931(2008).

44. Y. Tomizawa, Y. Sekido, M. Kondo, B. Gao, J. Yokota, J. Roche, H. Drabkin, M. I. Lerman, A. F. Gazdar, J. D. Minna, Inhibition of lung cancer cell growth and induction of apoptosis after reexpression of 3p21.3 candidate tumor suppressor gene SEMA3B. Proc. Natl. Acad. Sci. U.S.A. 98, 13954–13959 (2001).

45. C. Tse, R. H. Xiang, T. Bracht, S. L. Naylor, Human Semaphorin 3B (SEMA3B) located at chromosome 3p21.3 suppresses tumor formation in an adenocarcinoma cell line. Cancer Res. 62, 542–546 (2002).

46. T. Kuroki, F. Trapasso, S. Yendamuri, A. Matsuyama, H. Alder, N. N. Williams, L. R. Kaiser, C. M. Croce, Allelic loss on chromosome 3p21.3 and promoter hypermethylation of semaphorin 3B in non-small cell lung cancer. Cancer Res. 63, 3352–3355 (2003).

47. E. Castro-Rivera, S. Ran, P. Thorpe, J. D. Minna, Semaphorin 3B (SEMA3B) induces apoptosis in lung and breast cancer, whereas $VEGF_{165}$ antagonizes this effect. Proc. Natl. Acad. Sci. U.S.A. 101, 11432–11437(2004).

48. P. Shahi, C.-Y. Wang, J. Chou, C. Hagerling, H. Gonzalez Velozo, A. Ruderisch, Y. Yu, M.-D. Lai, Z. Werb,GATA3 targets semaphorin 3B in mammary epithelial cells to suppress breast cancer progression and metastasis. Oncogene 36, 5567–5575 (2017).

49. A. D. Sabag, T. Smolkin, Y. Mumblat, M. Ueffing, O. Kessler, C. J. Gloeckner, G. Neufeld, The role of the plexin-A2 receptor in Sema3A and Sema3B signal transduction. J. Cell Sci. 127, 5240–5252 (2014).

50. Y. Wang, H. He, N. Srivastava, S. Vikarunnessa, Y.-b. Chen, J. Jiang, C. W. Cowan, X. Zhang, Plexins are GTPase-activating proteins for Rap and are activated by induced dimerization. Sci. Signal. 5, ra6 (2012).

51. Y. Wang, H. G. Pascoe, C. A. Brautigam, H. He, X. Zhang, Structural basis for activation and non-canonical catalysis of the Rap GTPase activating protein domain of plexin. eLife 2, e01279 (2013).

52.T. Sakai, T. Furuyama, Y. Ohoka, N. Miyazaki, S.h. Fujioka, H. Sugimoto, M. Amasaki, S. Hattori, T.Matsuya, S. Inag aki, Mouse semaphorin H induces PC12 cell neurite outgrowth activating Ras-mitogen-activated protein kinase signaling pathway via Ca^{2+} influx. J. Biol. Chem. 274, 29666–29671 (1999).

53. J. K. Atwal, K. K. Singh, M. Tessier-Lavigne, F. D. Miller, D. R. Kaplan, Semaphorin 3F antagonizes neurotrophin-induced phosphatidylinositol 3-kinase and mitogen-activated protein kinase kinase signaling: A mechanism for growth cone collapse. J. Neurosci. 23, 7602–7609 (2003).

54. V. A. Potiron, G. Sharma, P. Nasarre, J. A. Clarhaut, H. G. Augustin, R. M. Gemmill, J. Roche, H. A. Drabkin,Semaphorin SEMA3F affects multiple signaling pathways in lung cancer cells. Cancer Res. 67, 8708–8715(2007).

55. D. S. Campbell, C. E. Holt, Chemotropic responses of retinal growth cones mediated by rapid local protein synthesis and degradation. Neuron 32, 1013–1026 (2001).

56. C. Guirland, S. Suzuki, M. Kojima, B. Lu, J. Q. Zheng, Lipid rafts mediate chemotropic guidance of nerve growth cones. Neuron 42, 51–62 (2004).

57. Q. Qin, G. Liao, M. Baudry, X. Bi, Role of calpain-mediated p53 truncation in semaphorin 3A-induced axonal growth regulation. Proc. Natl. Acad. Sci. U.S.A. 107, 13883–13887 (2010).

58.N.K. Hanchate, P. Giacobini, P. Lhuillier, J. Parkash, C. Espy, C. Fouveaut, C. Leroy, S. Baron, C. Campagne,C. Van acker, F. Collier, C. Cruaud, V. Meyer, A. GarcíaPiñero, D. Dewailly, C. CortetRudelli, K. Gersak, C.Metz, G. Chabrier, M . Pugeat, J. Young, J.-P. Hardelin, V. Prevot, C. Dodé, SEMA3A, a gene involved in axonal pathfinding, is mutated in patients with Kallmann syndrome. PLOS Genet. 8, e1002896 (2012).

59. R. P. Kruger, J. Aurandt, K.-L. Guan, Semaphorins command cells to move. Nat. Rev. Mol. Cell Biol. 6,789–800 (2005).

60. H. Jung, B. C. Yoon, C. E. Holt, Axonal mRNA localization and local protein synthesis in nervous system assembly, maintenance and repair. Nat. Rev. Neurosci. 13, 308–324 (2012).

61.M.-E. Gilles, F. Maione, M. Cossutta, G. Carpentier, L. Caruana, S. Di
Maria, C. Houppe, D. Destouches, K.Shchors, C. Prochasson, F. Mongelard, S. Lamba, A. Bardelli, P. Bouvet, A. Couvel ard, J. Courty, E. Giraudo, I.Cascone, Nucleolin targeting impairs the progression of pancreatic cancer and promotes the normalization of tumor vasculature. Cancer Res. 76, 7181–7193 (2016).

62. R. D. Jager, W. F. Mieler, J. W. Miller, Age-related macular degeneration. N. Engl. J. Med. 358, 2606–2617(2008).

63. V. Lambert, J. Lecomte, S. Hansen, S. Blacher, M.-L. A. Gonzalez, I. Struman, N. E. Sounni, E. Rozet, P. de Tullio, J.-M. Foidart, J.-M. Rakic, A. Noel, Laser-induced choroidal neovascularization model to study age-related macular degeneration in mice. Nat. Protoc. 8, 2197–2211 (2013).

64. H.-B. Pang, G. B. Braun, T. Friman, P. Aza-Blanc, M. E. Ruidiaz, K. N. Sugahara, T. Teesalu, E. Ruoslahti, An endocytosis pathway initiated through neuropilin-1 and regulated by nutrient availability. Nat. Commun. 5,4904 (2014).

65. A. E. Fournier, F. Nakamura, S. Kawamoto, Y. Goshima, R. G. Kalb, S. M. Strittmatter, Semaphorin3A enhances endocytosis at sites of receptor–F-actin colocalization during growth cone collapse. J. Cell Biol.149, 411–422 (2000).

66. M. Piper, S. Salih, C. Weinl, C. E. Holt, W. A. Harris, Endocytosis-dependent desensitization and protein synthesis–dependent resensitization in retinal growth cone adaptation. Nat. Neurosci. 8, 179–186 (2005).

67.K. Zylbersztejn, M. Petkovic, A. Burgo, M. Deck, S. Garel, S. Marcos, E. BlochGallego, F. Nothias, G.Serini, D. Bagna rd, T. Binz, T. Galli, The vesicular SNARE Synaptobrevin is required for Semaphorin 3A axonal repulsion. J. Cell Biol. 196, 37–46 (2012).

68.S. LeJan, M. Hayashi, Z. Kasza, I. Eriksson, J.R. Bishop, I. Weibrecht, J. Heldin, K. Holmborn, L.Jakobsson, O. Söde rberg, D. Spillmann, J. D. Esko, L. Claesson-Welsh, L. Kjellén, J. Kreuger, Functional overlap between chondroitin and heparan sulfate proteoglycans during VEGF-induced sprouting angiogenesis. Arterioscler. Thromb. Vasc. Biol. 32, 1255–1263 (2012).

69. F. de Winter, J. C. F. Kwok, J. W. Fawcett, T. T. Vo, D. Carulli, J. Verhaagen, The chemorepulsive protein Semaphorin 3A and perineuronal net-mediated plasticity. Neural Plast. 2016, 3679545 (2016).

70. R. O. Hynes, Q. Zhao, The evolution of cell adhesion. J. Cell Biol. 150, F89–F96 (2000).

71. I. Garrido-Laguna, M. Hidalgo, Pancreatic cancer: From state-of-the-art treatments to promising novel therapies. Nat. Rev. Clin. Oncol. 12, 319–334 (2015).

72. L. A. Kelley, S. Mezulis, C. M. Yates, M. N. Wass, M. J. E. Sternberg, The Phyre2 web portal for protein modeling, prediction and analysis. Nat. Protoc. 10, 845–858 (2015).

73.B. Hess, C. Kutzner, D. van der Spoel, E. Lindahl, GROMACS 4: Algorithms for highly efficient, load-balanced, and scalable molecular simulation. J. Chem. Theory Comput. 4, 435–447 (2008).

74. K. Lindorff-Larsen, S. Piana, K. Palmo, P. Maragakis, J. L. Klepeis, R. O. Dror, D. E. Shaw, Improved side-chain torsion potentials for the Amber ff99SB protein force field. Proteins 78, 1950–1958 (2010).

75. G. M. Sastry, M. Adzhigirey, T. Day, R. Annabhimoju, W. Sherman, Protein and ligand preparation: Parameters, protocols, and influence on virtual screening enrichments. J. Comput. Aided Mol. Des. 27,221–234 (2013).

76. G. A. Kaminski, R. A. Friesner, J. Tirado-Rives, W. L. Jorgensen, Evaluation and reparametrization of the OPLS-AA force field for proteins via comparison with accurate quantum chemical calculations on peptides.J. Phys. Chem. B 105, 6474–6487 (2001).

77. W. L. Jorgensen, J. Chandrasekhar, J. D. Madura, R. W. Impey, M. L. Klein, Comparison of simple potential functions for simulating liquid water. J. Chem. Phys. 79, 926–935 (1983).

78. A. Cheng,K. M. Merz Application of the nosé–hoover chain algorithm to the study of protein dynamics. J. Phys. Chem. 100, 1927–1937 (1996).

79. H. J. C. Berendsen, J. P. M. Postma, W. F. van Gunsteren, A. DiNola, J. R. Haak, Molecular dynamics with coupling to an external bath. J. Chem. Phys. 81, 3684–3690 (1984).

80. G. Bussi, D. Donadio, M. Parrinello, Canonical sampling through velocity rescaling. J. Chem. Phys. 126,014101 (2007).

81. M. Parrinello, A. Rahman, Polymorphic transitions in single crystals: A new molecular dynamics method. J. Appl. Phys. 52, 7182–7190 (1981).

82. S. Páll, B. Hess, A flexible algorithm for calculating pair interactions on SIMD architectures. Comput. Phys. Commun. 184, 2641–2650 (2013).

83. T. A. Darden, D. M. York, L. G. Pedersen, Particle mesh Ewald: An N·log(N) method for Ewald sums in large systems. J. Chem. Phys. 98, 10089–10092 (1993).

84. B. Hess, H. Bekker, H. J. C. Berendsen, J. G. E. M. Fraaije, LINCS: A linear constraint solver for molecular simulations. J. Comput. Chem. 18, 1463−1472 (1997).

85. W. Humphrey, A. Dalke, K. K. Schulten, VMD: Visual molecular dynamics. J. Mol. Graph. 14, 33–38 (1996).

86. L. Tamagnone, S. Artigiani, H. Chen, Z. He, G.-l. Ming, H.-j. Song, A. Chedotal, M. L. Winberg, C. S. Goodman,M.-m. Poo, M. Tessier-Lavigne, P. M. Comoglio, Plexins are a large family of receptors for transmembrane, secreted, and GPI-anchored semaphorins in vertebrates. Cell 99, 71–80 (1999).

87. G. Bergers, K. Javaherian, K.-M. Lo, J. Folkman, D. Hanahan, Effects of angiogenesis inhibitors on multistage carcinogenesis in mice. Science 284, 808–812 (1999).

88.M. PàezRibes,E. Allen, J. Hudock, T. Takeda, H. Okuyama, F. Viñals, M. Inoue, G. Bergers, D. Hanahan, O.Casanovas, Antiangiogenic therapy elicits malignant progression of tumors to increased local invasion and distant metastasis. Cancer Cell 15, 220–231 (2009).

89. F. Montassar, M. Darche, A. Blaizot, S. Augustin, J.-B. Conart, A. Millet, M. Elayeb, J.-A. Sahel, A. Réaux-Le Goazigo, F. Sennlaub, N. Marrakchi, E. Messadi, X. Guillonneau, Lebecetin, a C-type lectin, inhibits choroidal and retinal neovascularization. FASEB J. 31, 1107–1119 (2017).

Acknowledgments: We thank D. Hanahan and K. Shchors (Swiss Institute for Experimental Cancer Research, École polytechnique fédérale de Lausanne, Lausanne, Switzerland), who made available $p48^{cre}$, $Kras^{LSL\_G12D}$, $p53^{R172H/+}$, and $Ink4a/Arf^{flox/+}$ cells. We acknowledge M. J. Humphries (Wellcome Trust Centre for Cell-Matrix Research, University of Manchester, UK) for providing the purified SNAKA51 mAb. Funding: This study was supported by Italian Association for Cancer Research (AIRC-IG grant nos. 13016 and 16702 to G.S., 15645 to E.G., and 15179 to L.T.), Fondazione

Piemontese per la Ricerca sul Cancro (FPRC)–ONLUS grant “MIUR 2010 Vaschetto-5 per mille 2010 MIUR” and “FPRC-5 per mille 2014 Ministero Salute” (to G.S., E.G., and L.T.), Associazione “Augusto per la Vita” (to G.S.), Swiss National Science Foundation (Sinergia grant no. CRSII3 160742/1 to E.G.), Ministero della Salute (grant no. RF-2011-02350836 to G.M.), Agence National de la Recherche grant “Normather” (to I.C.), Fondazione Telethon (grant no. GGP15098 to M. Giustetto), Albero di Greta ONLUS (to M. Giustetto), and International Foundation for CDKL5 Research (to M. Giustetto). C.C. was supported, in part, by the Giulio Dalbesio Memorial Cancer Research Fellowship, in partnership with Associazione Augusto per la Vita. N.M. was supported by a fellowship from Fondazione Telethon (grant no. GGP15098). Author contributions: G.S., E.G., and L.T. conceived the project. G.S., E.G., L.T., G.M., I.C., M. Giacca, M. Giustetto, N.G., F.M., C.C., M. Ghitti, D.V., N.M., M.D., G.C., and Y.Q. designed the experiments. L.Z. and M. Giacca provided the key reagents. N.G., F.M., L.T., C.C., M. Ghitti, D.V., N.M., M.D., G.C., and Y.Q. performed the experiments. G.S., E.G., L.T., G.M., I.C., M. Giacca, M. Giustetto, N.G., F.M., C.C., M. Ghitti, D.V., N.M., and M.D. analyzed the data. G.S., E.G., L.T., G.M., I.C., M. Giacca, M. Giustetto, N.G., F.M., C.C., M. Ghitti, D.V., N.M., and M.D. interpreted the results. G.S., E.G., L.T., G.M., I.C., M. Giacca, M. Giustetto, N.G., F.M. and M. Ghitti wrote the manuscript. All authors read and approved the manuscript. Competing interests: G.S., E.G., and L.T. are inventors of a pending patent application on “Non-natural semaphorins 3 and their medical use” (international application no. PCT/EP2016/053750) related to this research. G.S., E.G., and L.T. are cofounders and shareholders of SeaGull Therapeutics SAS. All other authors declare that they have no competing interests.